

Thin-film ferroelectric materials and their applications

Lane W. Martin^{1,2} and Andrew M. Rappe³

Abstract | Ferroelectric materials, because of their robust spontaneous electrical polarization, are widely used in various applications. Recent advances in modelling, synthesis and characterization techniques are spurring unprecedented advances in the study of these materials. In this Review, we focus on thin-film ferroelectric materials and, in particular, on the possibility of controlling their properties through the application of strain engineering in conventional and unconventional ways. We explore how the study of ferroelectric materials has expanded our understanding of fundamental effects, enabled the discovery of novel phases and physics, and allowed unprecedented control of materials properties. We discuss several exciting possibilities for the development of new devices, including those in electronic, thermal and photovoltaic applications, and transduction sensors and actuators. We conclude with a brief survey of the different directions that the field may expand to over the coming years.

The modern era^{1–3} for ferroelectricity can be traced back to the Second World War, which gave an impetus to the development of advanced functional materials for a range of applications (such as the sonar) and to the synthesis of new materials (for example, ABO₃ perovskites such as BaTiO₃). In the following years, new phenomenological theories were formulated to describe ferroelectric materials with great accuracy, and countless applications leveraged bulk versions of these materials. By the 1960s, initial studies of ferroelectric films were undertaken to realize non-volatile memories, but difficulty in producing high-quality films limited their use until the 1980s. By the 1990s, ferroelectrics (films in particular) were finding widespread application in memories, radio frequency and microwave devices, pyroelectric (thermal) and piezoelectric (stress) sensors and actuators, and in many other systems.

The past decade has seen unprecedented advances in theoretical and computational models, synthesis and characterization, allowing researchers to probe ferroelectric materials across a huge range of lengths and timescales. Quantum-mechanical modelling has provided dramatic insight into the physical properties of ferroelectrics, and the modern theory of polarization has revolutionized the understanding of this class of materials⁴. Today, a range of clever modelling techniques spans from angstrom and femtosecond scales to macroscopic phenomenology⁵. This allows insight-driven and massively parallel design of new materials and heterostructures. Simultaneously, advances in synthesis, thin-film-based methodologies in particular, have enabled

unprecedented control of the resulting materials^{6,7}. It is now possible to finely control cation/anion chemistries and defect structures, to apply large strains via epitaxial lattice mismatch with a substrate, and to create artificial heterostructures engineered down to the unit cell, which enable new states of matter and phenomena. Advances in characterization have also unlocked new understanding. Electron and scanning-probe microscopy techniques provide atomic-scale spatially resolved images of structure, *in situ* and *in operando* studies probe the nature of switching in real time, and advanced optical and structural probes reveal ultrafast responses⁸. Here, we review numerous advances made in the past decade, examining how they have changed our understanding of the physics of ferroelectric materials, and we discuss how to use and apply these materials in novel ways.

Thin-film phenomena and strain control

Any lattice composed of oppositely charged species (that is, cations and anions) relies on short-range interactions between adjacent electron clouds to stabilize its structure. In ferroelectric materials (BOX 1), these interactions result in the formation of a double-well potential that stabilizes a distorted structure over a symmetric one. For example, in ferroelectrics such as PbTiO₃ and BaTiO₃, the Ti 3*d*–O 2*p* orbital hybridization is essential for stabilizing the distorted ferroelectric phase⁹. Owing to the strong coupling between the electronic order parameter (polarization) and the charge and lattice degrees of freedom in ferroelectrics, changing the electrical and elastic boundary conditions can have a direct

¹Department of Materials Science and Engineering, University of California, Berkeley, California 94720, USA.

²Materials Science Division, Lawrence Berkeley National Laboratory, Berkeley, California 94720, USA.

³The Makineni Theoretical Laboratories, Department of Chemistry, University of Pennsylvania, Philadelphia 19104, USA.

Correspondence to L.W.M. lwmartin@berkeley.edu

Article number: 16087
doi:10.1038/natrevmats.2016.87
Published online 15 Nov 2016

(and dramatic) effect on ferroelectricity. It is now possible to deterministically tip the balance between the various factors that determine the equilibrium structure, such as the electrostatic (or depolarization), domain wall, and gradient energies, and the polarization. For example, biaxial strain, which emerges when a film is clamped to a substrate but free in the out-of-plane direction, can

dramatically affect the film properties. Although ferroelectric oxides are brittle and crack or deform under moderate tensile or compressive strains ($\sim 0.1\%$)^{10,11}, their thin-film counterparts can withstand biaxial strains of $\pm 3\%$ — the record to date is a 6% compressive strain in BiFeO₃/YAlO₃ (110)^{12,13}. Epitaxial strain allows researchers to mimic conditions observed deep within the Earth, because a 1% lattice mismatch strain is roughly equivalent to the application of 1–10 GPa of pressure or to a depth of 30–40 km below the surface of the Earth. Attaining these effective pressures allows access to a host of different phases, polymorphs and properties.

Box 1 | Materials hierarchy and important definitions

All materials (32 crystal classes)

All materials exhibit electrostriction, which is the elastic strain induced by the application of an electric field (E) that is quadratic in nature. Insulating materials are additionally dielectric, meaning that the material undergoes small rearrangements of charge and exhibits a transient electric polarization under the application of an electric field. Finally, all materials are flexoelectric and polarize if subjected to an inhomogeneous deformation (bending), which can break centrosymmetry and induce a polarization.

Piezoelectric materials (20 crystal classes)

A subset of materials for which the application of stress induces an electric potential or, conversely, the application of an electric field induces mechanical strain through the so-called converse piezoelectric effect.

Polar or pyroelectric materials (10 crystal classes)

Some piezoelectric materials possess a polar axis and develop a spontaneous polarization (P): thus, they are called polar. Polarization can undergo temperature-dependent changes that result in a flow of charge in a circuit connecting the surfaces of the crystal; therefore, these materials are also called pyroelectrics.

Ferroelectric materials

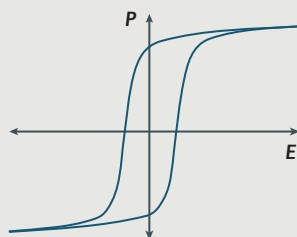
Some polar or pyroelectric materials possess two or more stable polarized states in the absence of an electric field, and the application of an electric field can induce switching between these states. The hysteretic response of ferroelectric materials is illustrated in panel a.

Typically, ferroelectric materials display ferroelectricity only below the Curie temperature (T_C), above which a paraelectric state is observed, associated with a high-symmetry structure (the aristotype; panel b, left). The phase transition can be either first- or second-order, as illustrated in panel c.

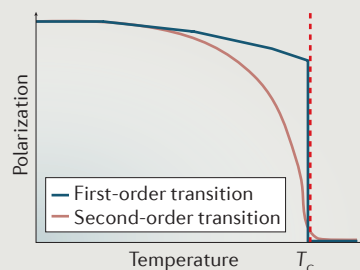
Ferroelastic materials

Ferroelectric materials can spontaneously order into domains (local regions of uniform polarization) separated by domain walls. Ferroelastic materials are a subset of ferroelectric materials, which exhibit two or more orientation states in the absence of mechanical stress (and an electric field) and can be shifted from one to another by mechanical stress.

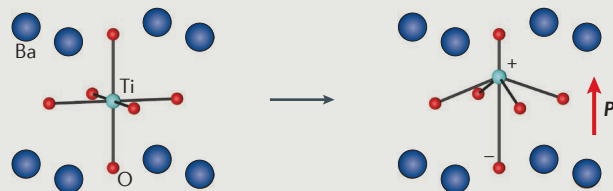
a Hysteretic response



c Phase transitions



b Aristotype and ferroelectric



Conventional thin-film strain effects

By the early 2000s, there were already numerous observations of intriguing phenomena in ferroelectric films originating from lattice-mismatch-based strain^{5,6}. The study of thin films provides information about the fundamental size limits for ferroelectricity. First-principles calculations predict a critical thickness of around six unit cells for BaTiO₃ films¹⁴, and synchrotron X-ray diffraction studies show that in PbTiO₃/SrTiO₃ (001) films the ferroelectric order is stable down to three unit cells¹⁵. Stabilizing ferroelectricity in ultrathin films is difficult, because incomplete screening at ferroelectric-metal interfaces can adversely affect the polarization^{16–18}. However, particular ferroelectric-metal combinations are predicted to support robust ferroelectricity down to the single-unit-cell thickness¹⁶; in such ultrathin films, adsorbed species and chemical passivation are critical for polarization stability^{19,20}. Ultimately, the imperfect screening of depolarization fields is a key factor in determining the ferroelectric size limit. Thus, to stabilize ferroelectricity in ultrathin films, materials must either form self-compensated periodic domain structures or decrease the magnitude of the polarization by locally adapting atomic displacements. The interface between the ferroelectric and the environment and/or contacts is also crucial¹⁶ in determining the critical thickness (the so-called dead layer)²¹.

Going beyond single-component ferroelectrics, two-²² and three-component^{23–25} superlattices with enhanced properties were proposed theoretically and then experimentally realized^{26–32}. An example are tricolour BaTiO₃/SrTiO₃/CaTiO₃ superlattices that, by coherently straining the BaTiO₃ layer and through heterointerfacial coupling, induce a 50% enhancement in the ferroelectric polarization³³ (FIG. 1a). Another example are PbTiO₃/SrTiO₃ superlattices, in which a new form of interfacial coupling is obtained based on antiferrodistortive rotations of the octahedra, wherein polarization resulting from the asymmetry in the rotation pattern is possible^{34,35}.

The effect of epitaxial strain on ferroelectrics has also been widely studied in thicker films. Early successful investigations probed the strong coupling between polarization and the charge and lattice degrees of freedom, shedding light on the epitaxial-strain-induced room-temperature ferroelectricity in SrTiO₃ (REF. 36) and on the enhancement of the transition temperature and remnant polarization in BaTiO₃ (REF. 37). Films of multiferroic BiFeO₃ (G-type antiferromagnetic and

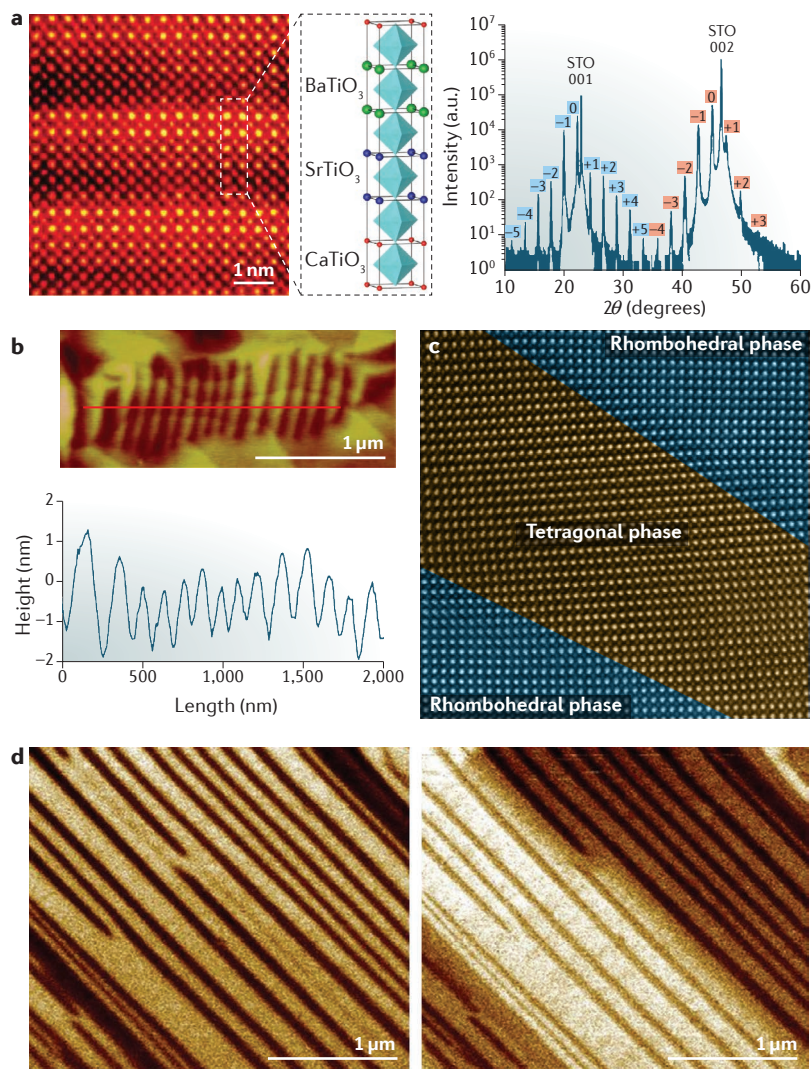


Figure 1 | Thin-film strain effects. **a** | Cross-sectional, atomic-scale Z-contrast image of the compositionally abrupt interface in the $\text{CaTiO}_3/\text{SrTiO}_3/\text{BaTiO}_3$ tri-colour superlattice, together with a schematic illustration of the structure (left). Wide-angle X-ray diffraction scan of the same superlattice showing high crystallinity, significant long-range periodicity and the superlattice peaks expected for such structures (right). The STO 001 and 002 peaks arise from the substrate SrTiO_3 ; the two sets of superlattice peaks are marked with blue and red numbers, respectively. **b** | High-resolution atomic force microscopy image of a mixed-phase region in highly-strained BiFeO_3 with the corresponding line profile along the red line, showing the 2–3-nm height changes observed when moving across the different phases in the material. **c** | High-resolution cross-sectional transmission electron microscopy image of the boundary between the rhombohedral- and tetragonal-like phases in the mixed-phase structure, showing smooth transitions and no defects despite the large change in lattice parameter. **d** | Vertical (out-of-plane; left) and lateral (in-plane; right) piezoresponse force microscopy images of a La-doped BiFeO_3 film grown on a DyScO_3 substrate revealing ordered, 109° domain-wall arrays. a. u., arbitrary units. Panel **a** is from REF. 33, Nature Publishing Group. Panels **b** and **c** are adapted with permission from REF. 12, AAAS. Panel **d** is adapted with permission from REF. 71, American Chemical Society.

ferroelectric)⁷ have been grown on essentially every available oxide substrate (from 7% compressive to 1.3% tensile strain), as well as on semiconductor wafers. Strain has been shown to change the easy direction of magnetization^{38,39} and stabilize new structural polymorphs. In particular, a new structure of BiFeO_3 was predicted^{40,41}

and subsequently observed with $P4mm$ symmetry, a huge $c/a \approx 1.26$ (the ratio of the long, $c = 4.655 \text{ \AA}$, to the short, $a = 3.665 \text{ \AA}$, axis of the unit cell) and a large spontaneous polarization^{42,43}. It is possible to produce films of this highly distorted tetragonal-like phase by applying large strains (approximately -4.5%), and it was observed that as the film thickness increases, so-called mixed-phase films exhibiting tetragonal- and rhombohedral-like phases form in complex stripe-like structures¹² (FIG. 1b). These mixed-phase structures, despite possessing a large formal lattice mismatch between the two phases, exhibit coherent interfaces owing to the gradually evolving lattice deformation (FIG. 1c). These structures also have a complex temperature- and thickness-dependent evolution; the tetragonal-like phase transforms into the mixed-phase structure via a process that resembles a strain-induced spinodal instability⁴⁴, the onset of which can be tuned by composition⁴⁵. Electric-field-dependent studies of mixed-phase structures revealed large electromechanical responses (4–5%) made possible by the motion of boundaries between the different phases^{46,47}. Further studies identified an intermediate monoclinic phase, in addition to the previously observed rhombohedral- and tetragonal-like phases, which bridges the two other phases and enables electric-field modulation^{48,49}. Strain has also provided a route for producing other novel polar and/or ferroelectric materials, including PbVO_3 (REFS 50,51) and EuTiO_3 (REF. 52).

Besides eliciting new polar structures, conventional, lattice-mismatch-induced thin-film strain has had an important role in controlling domain structures in ferroelectric materials. Domains form as a consequence of the competition between elastic, electrostatic, gradient and domain-wall energies, and are important for material properties^{53,54}. For example, in Ti-rich $\text{PbZr}_{1-x}\text{Ti}_x\text{O}_3$, it has long been known that polydomain structures can form, with compressive strain favouring monodomains polarized out-of-plane (c domains) and reduced compressive or tensile strain favouring multidomain $c/a/c/a$ structures (alternating domains of type c and a , polarized respectively out-of-plane and in-plane and separated by 90° domain walls)⁵⁵. Extensive phenomenological modelling of this and other systems has allowed the elaboration of phase diagrams for the strain evolution of domain structures^{56–58}. Recently, combined theoretical and experimental approaches demonstrated the possibility of deterministically controlling 90° domain structures in (001)-oriented $\text{PbZr}_{0.2}\text{Ti}_{0.8}\text{O}_3$ heterostructures; this control was used to explore the contribution of ferroelastic domain walls to dielectric permittivity and pyroelectricity^{59–63}. In the case of BiFeO_3 , which in its bulk form is a rhombohedral material, domain structures in (001)-oriented films exhibit either $\{100\}_{\text{pc}}$ or $\{101\}_{\text{pc}}$ (where pc denotes pseudocubic notation) domain boundaries and stripe patterns of energetically degenerate domains of equal width, which can be tuned with film orientation, elastic constraints and electrical boundary conditions. By balancing elastic and electrostatic energies, researchers have experimentally obtained 1D nanoscale domain arrays^{64–67}, controlled polarization variant selection^{68–70} and equilibrium domain structures⁷¹ (FIG. 1d).

Such control has enabled a range of exciting observations, including the correlation of different domain structures to variations in remanent polarization⁷², domain effects on fatigue lifetimes⁷³, deterministic control of switching pathways⁷⁴ and other effects⁷⁵.

Unconventional strain control

Researchers today are exploring the limits of what can be achieved using strain, while at the same time trying to overcome several limitations associated with traditional

strain control. These include limits in the amount of strain that can be applied before relaxation takes place (typically 1–2%), in the film thickness needed to maintain coherency — above these limits strain relaxation occurs, yielding films so thin that they are unsuitable for high-voltage applications — and in the available substrates, which hamper the tunability of the strain state. These limitations put stringent restrictions on our ability to manipulate and enhance the performance of ferroelectric materials. With this in mind, researchers have explored the use of thermal mismatch strain⁷⁶, anisotropic in-plane strain^{77,78} and nanostructuring, along with other approaches, to create enhanced strain⁷⁹.

Varying the chemical composition is a time-honoured route to enable the manipulation of material properties, and researchers are discovering that there are systems in which chemistry can have a major role in property control. For example, rare-earth-alloying of BiFeO₃ leads to a feature resembling a morphotropic phase boundary with a rhombohedral-to-orthorhombic structural phase transition, which is associated with a substantial enhancement in dielectric and piezoelectric properties. Different studies have revealed a universal behaviour at this boundary, independent of the rare-earth species: the structural and functional properties can be described with the averaged A-site ionic radius as the primary control parameter^{80–84}. At the same time, there is growing evidence that even small changes in the chemistry and defect structures of complex oxides can affect their properties^{85–91}. By investigating anomalously large lattice expansions in BaTiO₃ films, researchers demonstrated that the growth process can be controlled to deterministically produce desired defect orientations. These defects possess both electric and elastic dipole moments that can couple to the polarization and epitaxial strain, giving rise to anisotropic lattice deformations and enhancing the ferroelectric transition temperature to over 1,000 °C (FIG. 2a,b). These results provide a potential pathway — apart from the use of oxide substrates — to strain-engineered materials⁹².

The vast majority of investigations on the epitaxial growth of ferroelectrics have focused on (001)-oriented films. However, changing the orientation of a film alters how strain is applied and has the potential to grant additional control of domain structures and properties; this potential has not yet been widely investigated. Studies of (111)-oriented PbZr_{0.2}Ti_{0.8}O₃ films have revealed two interesting effects^{93–95}. First, (111)-oriented films exhibit high-density, nanotwinned domain structures made entirely of 90° domain walls and an enhanced dielectric permittivity that cannot be explained using traditional models. Subsequent studies revealed and quantified a ‘stationary’, or frozen, contribution to the permittivity up to 80 times larger than the bulk response, which arises from within the finite width of the domain walls. Under higher applied fields, experiments and molecular dynamics simulations revealed the presence of 180° and multistep 90° switching processes in (001)- or (101)- and (111)-oriented films, respectively. Although the nucleation-and-growth process behind 180° switching events is well understood, little evidence for 90°-switching-mediated domain reversal had been presented before^{96,97}.

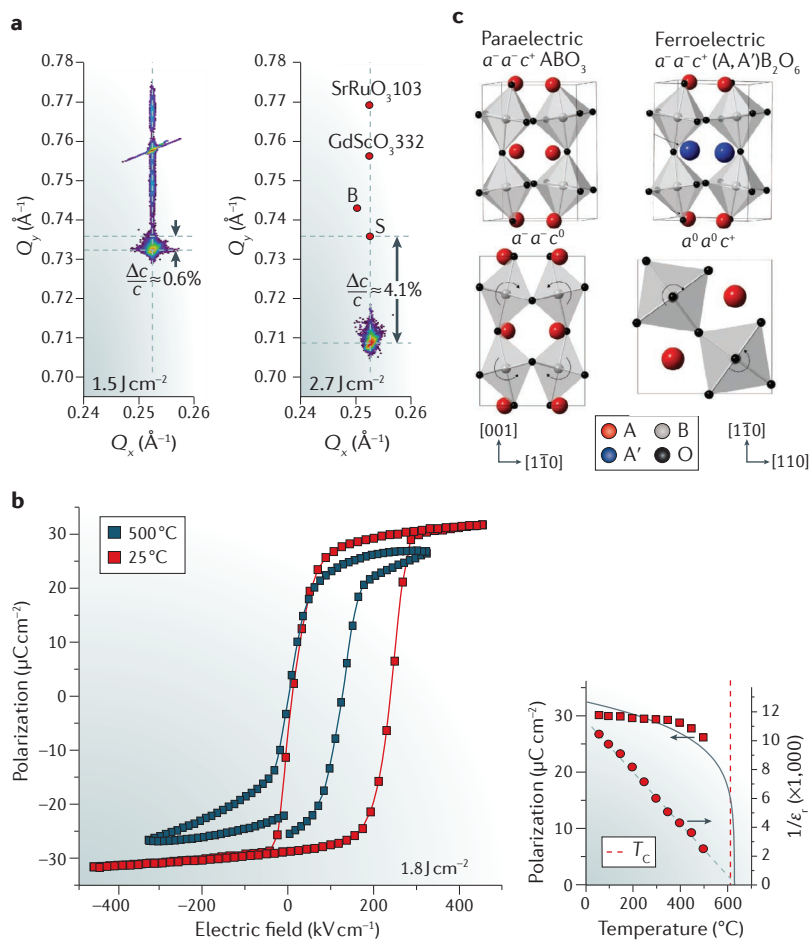


Figure 2 | Examples of the application of unconventional strain. a | X-ray reciprocal-space maps showing the 103- and 332-diffraction conditions of BaTiO₃ films grown on SrRuO₃ and GdScO₃ substrates, respectively, at a laser fluence of 1.5 J cm⁻² (left) and 2.7 J cm⁻² (right). If the growth conditions are tuned, coherently strained films with tunable lattice expansion going from Δc/c < 1% to Δc/c > 4% can be obtained (where c is the lattice parameter, and Q_x and Q_y are the reciprocal-space wave vector components along the x and y directions, respectively). **b** | These lattice-expanded films exhibit an enhanced ferroelectric transition temperature (T_C). For example, films grown at a laser fluence of 1.8 J cm⁻² exhibiting an additional lattice expansion of 1.4% remain ferroelectric up to temperatures above 600 °C. The larger graph (left) shows polarization–electric field hysteresis loops at room temperature and 500 °C, and the smaller graph (right) shows the polarization and the inverse permittivity (1/ε) as a function of temperature. **c** | Schematic representations of how octahedral rotations can induce ferroelectricity. The paraelectric Pnma structure (with Glazer rotation pattern a⁻a⁻c⁺) of the ABO₃ phase is shown, as well as the ferroelectric (A,A')B₂O₆ structure with the same a⁻a⁻c⁺ rotation. For completeness, the other a⁻a⁻c⁰ and a⁰a⁰c⁺ rotations for the Pnma structure are shown. Panels **a** and **b** are adapted with permission from REF. 92, Wiley. Panel **c** is adapted with permission from REF. 100, Wiley.

In films, the 90° domain switching process is typically too costly from the energetic point of view (because of substrate clamping), but in (111)-oriented films the modified domain structure and elastic boundary conditions make the 90° switching process⁵⁴ possible. This 90°-switching-mediated domain reversal enables faster switching that requires lower fields to be initiated.

Moving beyond film-substrate lattice mismatch, there is growing evidence that interfacial atomic and electronic structures are central to understanding how epitaxy affects the properties of a material. In 2011, a first-principles calculation demonstrated a new route to ferroelectricity, showing that oxygen octahedral rotations in perovskite (and related) structures can induce ferroelectricity⁹⁸. In this work, it was realized that some static rotational distortions of the octahedra can be considered as the combination of two nonpolar optic modes with different symmetries and can, in turn, induce hybrid improper ferroelectricity⁹⁹. Building on this observation, researchers proposed other routes to produce ferroelectricity, including one mechanism in which a spontaneous and switchable polarization emerges from the destabilization of antiferroelectricity; this occurs as a result of octahedral rotations and of the presence of ordered cation sublattices¹⁰⁰ (FIG. 2c). In a similar way, there is growing interest in using similarities (and differences) in symmetry, chemistry and octahedral rotations at interfaces to engineer ferroelectric order. For example, in BiFeO₃/La_{0.7}Sr_{0.3}MnO₃ heterostructures, the out-of-plane direction of polarization can be controlled simply by adjusting the termination of the La_{0.7}Sr_{0.3}MnO₃ layer from La_{0.7}Sr_{0.3}O to MnO₂ (REFS 101–103). These observations are thought to be related to the interfacial valence mismatch that, in turn, influences the electrostatic potential step across the interface, setting the preferred polarization direction. Atomic-resolution imaging has explored the evolution of lattice parameters and oxygen octahedral rotations across these ferroelectric-electrode interfaces and, for the first time, has demonstrated mesoscopic antiferrodistortive phase transitions near the interface in BiFeO₃ and corresponding variations in the electronic properties in adjacent layers^{104,105}. Advances in this field are aided by better ways of probing and quantifying minute local distortions, and stimulate the search for new ways of inducing such octahedral rotations to gain deterministic control of ferroelectrics. One example is the recent work¹⁰⁶ on BiFeO₃, in which the monoclinic distortion of a scandate substrate, resulting from oxygen octahedral rotations, is the driving force for domain variant selection. Researchers highlighted the importance of ‘symmetry mismatch’ on domain formation, showing that two-variant stripe domains are observed in films grown directly on DyScO₃, whereas four-variant domains are formed in films grown on SrTiO₃-buffered DyScO₃ with a thickness of at least 2 nm for the SrTiO₃ layer.

So far we have considered homogeneous strain, but in recent years there has been a re-emergence of interest in strain-graded ferroelectrics and flexoelectricity. Flexoelectricity — the coupling between polarization and strain gradients — is controlled by a fourth-rank tensor

and is allowed in all materials^{107,108}. Recently, attention in this field has focused on a better quantification of flexoelectric coefficients, including the formulation of first-principles theories^{109–111} and an examination of the large discrepancies between theoretical and experimental values¹¹². In general, the largest flexoelectric coefficients have been reported in ferroelectric films in which inhomogeneous strain relaxation^{113,114}, applied mechanical stress¹¹⁵, defect and domain engineering^{116–118}, and compositional gradients^{119–121} result in strain gradients larger than 10⁵ m⁻¹. In turn, flexoelectricity (and other related effects) can alter the response of materials, allowing for mechanically induced ferroelectric switching, driving horizontal shifts of ferroelectric hysteresis loops¹¹⁹ and enabling independent tuning of typically coupled ferroelectric susceptibilities^{113,119–121}. Researchers have successfully synthesized coherently strained, compositionally graded heterostructures that change from PbZr_{0.2}Ti_{0.8}O₃ (tetragonal) at the substrate interface to PbZr_{0.8}Ti_{0.2}O₃ (rhombohedral) at the film surface with a strain gradient of ~4 × 10⁵ m⁻¹. The strain gradient is so large that the films exhibit tetragonal-like crystal and domain structures, despite half of the film having a composition on the rhombohedral side of the bulk phase diagram, and show a strong polarization response, albeit shifted along the voltage axis such that only one polarization state is stable. This built-in potential in turn reduces the low-field dielectric permittivity to that of monodomain films or even lower^{119,122}. The evolution of the built-in potential was shown to have a non-intuitive dependence on thickness, chemistry and relaxation, suggesting that more than just strain gradients are relevant¹²¹. Other routes to produce strain gradients include the use of scanning probe systems, whereby stress gradients, which can drive mechanically induced polarization switching¹¹⁵, can be generated using the tip, and microelectromechanical systems, in which bending can be applied to obtain on-demand strain gradients¹²³.

Thermal-based applications

The vast majority of work on thin-film ferroelectrics has focused on their potential for electric-field-based (that is, dielectric response, switching and actuation) and stress-based (that is, transduction) applications. Considerably less attention has been given to the study of their thermal responses, despite the underlying physics, which is complex and not fully understood, and the potential for applications. In the thermal realm, there are two major effects: the pyroelectric effect — the generation of a temporary electrical potential when a material is heated or cooled, arising from temperature-dependent changes in the polarization and from the resulting flow of charges to or from the surface of a crystal — and the electrocaloric effect — the change in temperature observed upon application of an external electric field under adiabatic conditions resulting from a change in entropy. These effects have been used in a range of applications, from infrared imaging to electron emission and from solid-state cooling to waste-heat energy conversion, and the field is now poised for a revolution made possible by advances in methodologies and understanding^{124–127}.

Large electrocaloric effects have been observed in $\text{PbZr}_{0.95}\text{Ti}_{0.05}\text{O}_3$ (REF. 128) (FIG. 3a), $(1-x)\text{PbMg}_y\text{Nb}_{1-y}\text{O}_3-x\text{PbTiO}_3$ (REFS 129,130) and $\text{SrBi}_2\text{Ta}_2\text{O}_9$ (REF. 131). The focus is now on routes to achieve even larger pyroelectric and electrocaloric effects. These efforts are aided by advanced modelling approaches, which have explored, for example, the role of domain walls and domain structure^{59,60}, film thickness and strain state^{132–134}, thermal-mismatch strains^{135,136}, chemical and other gradients¹³⁷, and multilayer structures^{138,139}. One study clarified the relative importance of different contributions to the pyroelectric response⁶², including intrinsic (arising from the response of the polarization within the domains), extrinsic (arising from the temperature-driven change in the domain structure) and secondary (arising from a temperature-driven, piezoelectric-induced change in the polarization) pyroelectric effects in $\text{PbZr}_{1-x}\text{Ti}_x\text{O}_3$ (FIG. 3b,c). New high-performance materials are also being developed, and large electrocaloric responses have been observed in antiferroelectrics near the field-induced antiferroelectric-to-ferroelectric transition^{140–142}, in BaTiO_3 single crystals near first-order phase transitions¹⁴³ (FIG. 3d), and in magnetoelectrically coupled $\text{La}_{0.7}\text{Ca}_{0.3}\text{MnO}_3/\text{BaTiO}_3$ (REF. 144). Recently, attention has turned to the deterministic design of high-performance materials for thermal applications. Examination of the figure of merit for various thermal applications reveals that performance optimization requires enhancing the pyroelectric coefficient and suppressing the dielectric permittivity, which is difficult considering that the dielectric and pyroelectric responses are generally both enhanced by chemistry-, temperature- and strain-driven structural phase transitions. In compositionally graded $\text{PbZr}_{1-x}\text{Ti}_x\text{O}_3$ thin films, it is possible to reduce the dielectric permittivity owing to a built-in electrostatic potential while maintaining a strong pyroelectric response, obtaining figures of merit more than four times larger than those in the commonly used material LiNbO_3 (REF. 120). This discovery could point towards new materials for applications such as infrared sensors, pyroelectric electron emitters and pyroelectric energy conversion systems^{145–147}.

The development of accurate probes for measuring pyroelectric and electrocaloric responses is important for the advancement of the field. In contrast to bulk materials, it is difficult to accurately measure the temperature changes during pyroelectric or electrocaloric studies in films. This had led to debates about the feasibility of implementing direct compared with indirect measurement techniques. Maxwell relations provide a convenient link between the entropy, S , and the displacement vector, \mathbf{D} (which is related to the polarization, \mathbf{P} , in ferroelectrics). Indirect measurements of the electrocaloric effect rely on measurements of $P(T)$, where T is the temperature, or, more conveniently, of dP/dT (the pyroelectric coefficient), followed by the application of the Maxwell relation to extract an estimate of the temperature change. Such indirect measurements require careful acknowledgement and understanding of the boundary conditions (especially the elastic ones), otherwise overestimation can occur. Direct measurements

are also difficult: devices are often very small, making thermocouple-based studies challenging, and the effects themselves can be very small and beyond the resolution of off-the-shelf instruments. Moreover, they can be susceptible to effects such as Joule heating from the current flowing through the material. Direct and indirect methods have been carefully compared, and although they can provide similar values for bulk materials, the results often significantly differ for clamped thin films^{148,149}. However, several new (or at least refined) measurement techniques for pyroelectric and electrocaloric effects have been reported in the past few years and will probably lead to new discoveries^{149–153}.

Moving beyond the pyroelectric and electrocaloric effects, ferroelectrics are also interesting for other thermal applications. For example, imperfect (oxygen non-stoichiometric) ferroelectrics could provide interesting thermoelectric responses near various ferroelectric and structural phase transitions^{154–156}. Studies on the tungsten bronzes (such as $(\text{Sr}, \text{Ba})_2\text{Nb}_2\text{O}_{6-x}$) show polarization-modulated conductivity, the appearance of Seebeck coefficients and of phonon scattering, as well as a thermoelectric figure of merit of ~ 1.4 (REFS 157–160). At the same time, there has been growing interest in how domain structures can be used to tune thermal conductivity. Recent studies have explored how domain walls can give rise to additional phonon scattering, reducing the thermal conductivity. It has been found that domain walls in BiFeO_3 have higher Kapitza resistance (interfacial thermal resistance) than most grain boundaries, reducing the overall thermal conductivity¹⁶¹. Because of their electric field dependence, these domain walls can be moved, changing the thermal conductivity¹⁶² (at the present time, by a modest 11%; FIG. 3e).

Advanced ferroelectric devices

In recent years, several promising developments in the use of ferroelectrics in new devices have been reported. For example, there has been considerable interest in the use of ferroelectric domain walls as device elements^{163,164}. Domain walls are known to, at times, exhibit properties that differ from those of the bulk; the best-known example is the observation of domain-wall conductivity in insulating ferroelectrics. Studies of BiFeO_3 revealed room-temperature electronic conductivity at domain walls¹⁶⁵ (FIG. 4a), which was ascribed to an increased carrier density resulting from an electrostatic potential step and a decrease in the bandgap within the wall^{166–168}. Conduction has been reported at all domain walls in BiFeO_3 (REF. 169) as well as at domain walls in $\text{PbZr}_{1-x}\text{Ti}_x\text{O}_3$ (REF. 170), BaTiO_3 (REF. 171), ErMnO_3 (REF. 172), HoMnO_3 (REF. 173) and LiNbO_3 (REF. 174). Further studies have probed the role of oxygen vacancies in the conduction behaviour^{175,176}, how domain-wall curvature can give rise to large conductivity changes ($\sim 500\%$)¹⁷⁷, how certain conducting domain walls in multiferroics can exhibit large magnetoresistance ($\sim 60\%$)¹⁷⁸, topological defect states and exotic properties in vortex domain structures¹⁷⁹, as well as memristor-like functionality¹⁸⁰. Efforts have also focused on controlling domain structures in devices. Using micro- and nanomachining, researchers showed

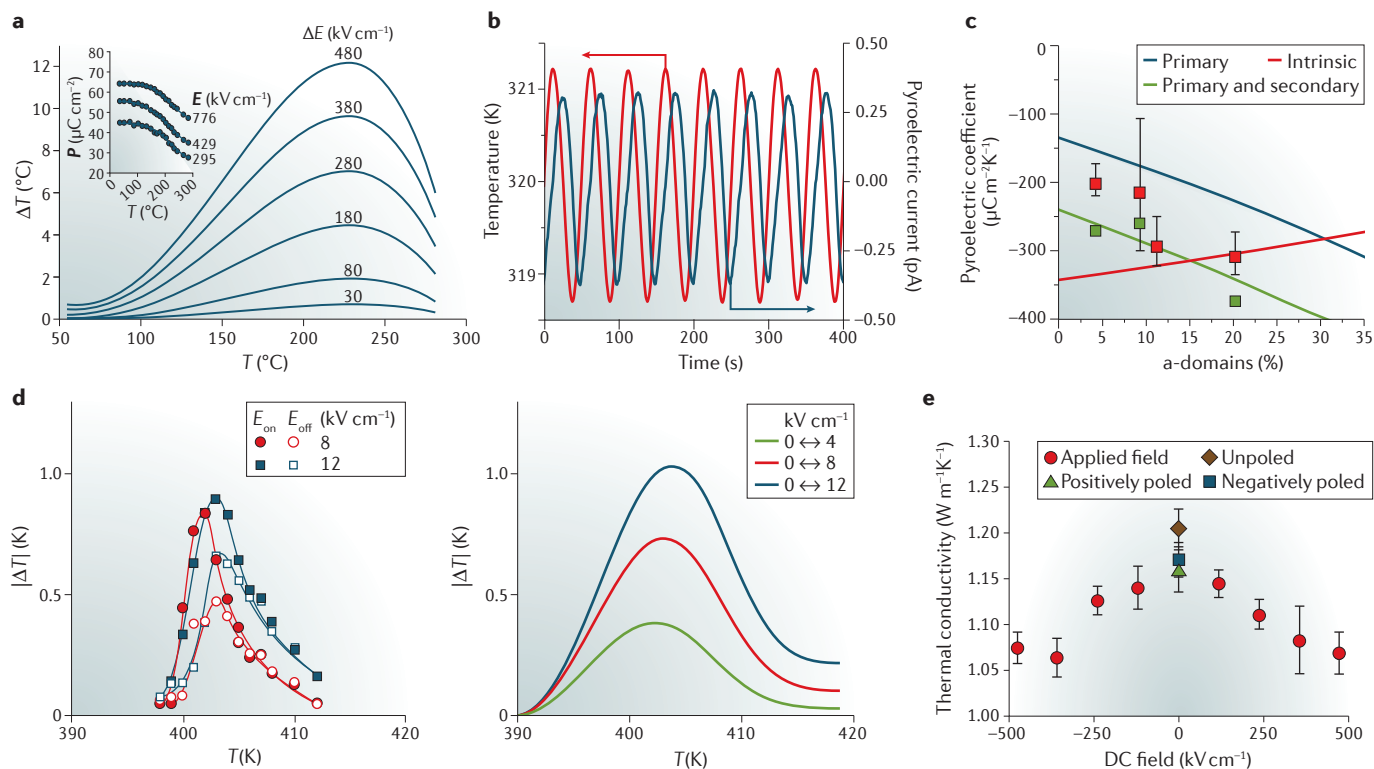


Figure 3 | Thermal properties of ferroelectric materials. **a** | Electrocaloric temperature change in $\text{PbZr}_{0.95}\text{Ti}_{0.05}\text{O}_3$ films extracted from indirect measurements and using the appropriate Maxwell relationship. The inset shows the measured polarization (P) as a function of temperature (T) for some values of the electric field (E). **b** | By applying a varying temperature profile (red curve) it is possible to use lock-in techniques to measure the corresponding pyroelectric current (blue curve). **c** | Information about the pyroelectric current can be used to extract the pyroelectric coefficient (red squares) that, in turn, can be compared to values from phenomenological theories (green squares) that include the primary and secondary (green line) effects for given strain states. This kind of analysis was used to show that the presence of domain walls and the thermal-expansion mismatch with the substrate are crucial for understanding the full response of materials such as $\text{PbZr}_{0.2}\text{Ti}_{0.8}\text{O}_3$. **d** | Directly measured electrocaloric temperature change in BaTiO_3 single crystals at different temperatures depending on the magnitude of the applied electric field (left) and indirectly measured electrocaloric temperature change for the same material under different applied electric fields (right). **e** | Dependence on the DC electric field of the thermal conductivity of $\text{PbZr}_{0.3}\text{Ti}_{0.7}\text{O}_3$ layers measured at room temperature (red data) together with the zero-field thermal conductivity of initially unpoled (grey diamond) and remanent, poled material after application of positive (green triangle) and negative (blue square) bias. Panel **a** is adapted with permission from REF. 128, AAAS. Panels **b** and **c** are adapted with permission from REF. 62, American Physical Society. Panel **d** is adapted with permission from REF. 143, Wiley. Panel **e** is adapted with permission from REF. 162, American Chemical Society.

deterministic domain production and motion under applied fields^{181,182}, making important progress towards domain-wall-based memristors and diode devices^{183,184}. Reliable and precise control of domain-wall generation, location and movement have also been demonstrated^{185,186}.

Apart from domain walls, there is considerable interest in the application of ferroelectrics in next-generation transistors, because their complex functionality makes them attractive for new low-power and non-volatile logic devices. One example is piezotronics: in piezoelectronic transistors an electrical input is transduced into an acoustic pulse by a piezoelectric element that, in turn, is used to drive a metal-to-insulator transition in a piezoresistive material¹⁸⁷. Piezoelectronic transistors could potentially offer an improvement of an order of magnitude in the voltage performance using 1/100th of the power compared with standard complementary metal-oxide-semiconductor field-effect

transistors (CMOS FETs). Another idea is to leverage electron tunnelling phenomena to produce new devices, similar to magnetic tunnel junctions, based on ferroelectrics^{188,189}. In such devices, the tunnelling electroresistance would arise from the influence of the polarization of the ferroelectric on the interface transmission function through changes in the electrostatic potential across the junction, in the interface bonding strength and/or in the strain associated with the piezoelectric response. The polarization-dependent control of tunnelling from scanning-probe tips¹⁹⁰, non-volatile memories with high on/off ratios¹⁹¹ and hybrid metal-ferroelectric-semiconductor junctions¹⁹² have already been reported. Another concept that is being investigated is that of negative capacitance. In short, a typical FET requires a change in the channel potential of at least 60 mV (at 300 K) to change the current by a factor of 10, which is the minimum for device operation.

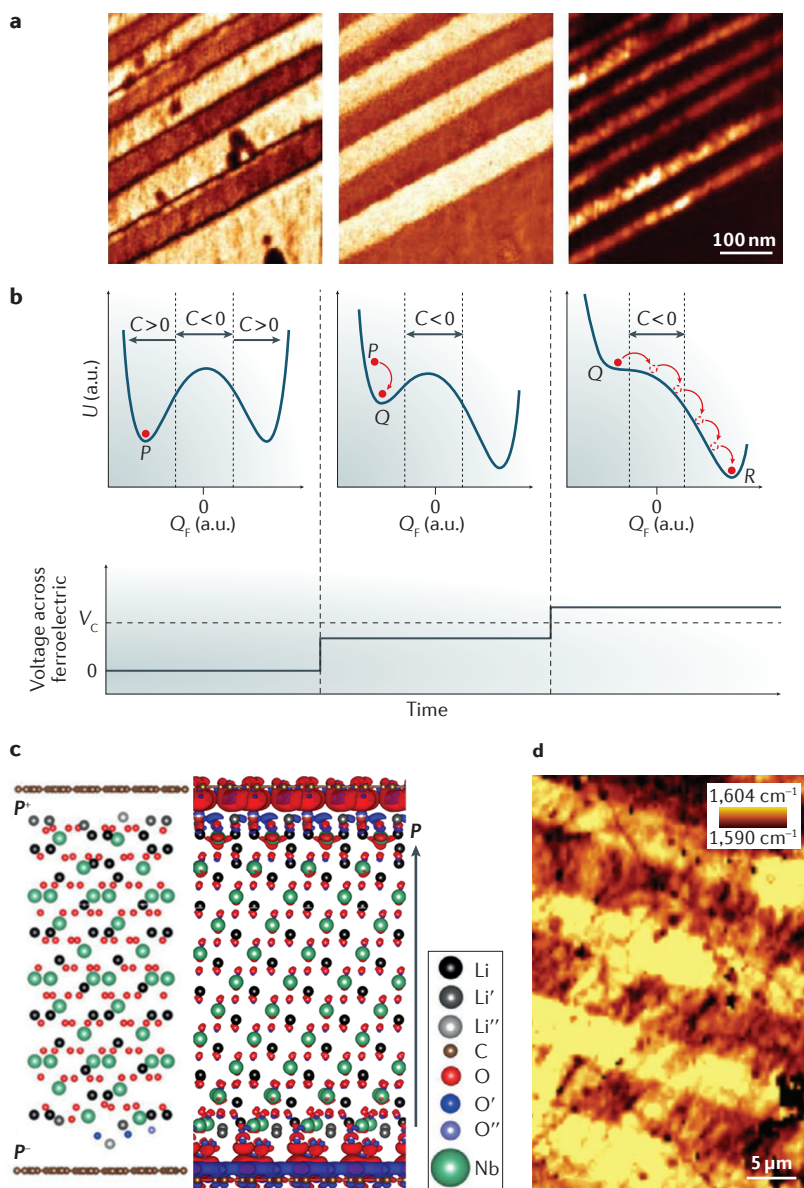


Figure 4 | Potential of ferroelectric materials for applications. **a** | Vertical piezoresponse force microscopy amplitude (left) and phase (middle) images of a 109° stripe domain-wall array in BiFeO_3 . The corresponding conducting atomic-force microscopy image showing conduction at each 109° domain wall is shown on the right. **b** | Potential energy (U) landscape description of negative capacitance (C) in ferroelectrics as a function of charge (Q_F). The left panel shows the case of a ferroelectric capacitor in the absence of an applied voltage: C is only negative in the barrier region between the energy minima. In the middle panel, an electric field is applied and the voltage is smaller than the coercive voltage (V_C) of the material. If the voltage is greater than V_C (right panel), the ferroelectric polarization descends through the negative C states. P , Q and R mark different polarization states. **c** | Atomic structure of a 2×1 surface-reconstructed LiNbO_3 slab with graphene adsorbed on both terminations; reconstructed adatoms and two trilayers ($\text{Li-O}_3\text{-Nb}$) near each interface are allowed to relax while the rest of the film is fixed to the polarization state at 298 K (left). Calculated electronic structure of the same graphene ferroelectric heterostructure with both up-polarized (top) and down-polarized (bottom) surfaces, which induce n- and p-doping in the graphene, respectively (right). **d** | Raman spectroscopy map of the graphene G-band frequency for a graphene/periodically-poled LiNbO_3 heterostructure in which the carrier density and doping state of the graphene are altered moving from up- to down-polarized domains. a.u., arbitrary units; P , polarization. Panel **a** is adapted with permission from REF. 176, American Physical Society; courtesy of J. Seidel, University of New South Wales, Australia. Panel **b** is from REF. 198, Nature Publishing Group. Panels **c** and **d** are from REF. 208, Nature Publishing Group.

A theoretical proposal suggested that by including a ferroelectric material in a standard FET geometry, this subthreshold slope might be surpassed using the concept of negative capacitance¹⁹³, leading to lower-power electronics (FIG. 4b). Detailed theoretical models¹⁹⁴ and experimental reports support this prediction, including studies on $\text{PbZr}_{0.2}\text{Ti}_{0.8}\text{O}_3/\text{SrTiO}_3$ bilayers in which the composite capacitance is larger than the SrTiO_3 capacitance¹⁹⁵, reports of room-temperature operation of negative capacitance^{196,197} and robust evidence for transient negative capacitance derived from a time-domain analysis of the switching process¹⁹⁸.

Considerable effort has also been devoted to the integration of 2D materials with ferroelectrics to manipulate carriers in the 2D material. In 2009, researchers found that the mobility of few-layer graphene FETs increased dramatically when they were integrated on $\text{PbZr}_{0.2}\text{Ti}_{0.8}\text{O}_3$ (REF. 199) and that a non-volatile memory could be realized²⁰⁰. Soon, more robust FETs were produced, a deeper understanding of the nature of the underlying interactions was developed and large resistance changes ($>500\%$)²⁰¹, as well as polarization-driven ferroelectric tunnel junction devices with tunnelling electroresistance greater than $6 \times 10^5\%$ ²⁰², were reported. At the same time, an odd hysteresis in the transfer curves of graphene was observed and attributed to slow dissociation and recombination dynamics of adsorbed water molecules^{203–205}. Ultimately, it was found that, depending on the environmental conditions and history of the devices, n- and p-type behaviour, as well as intrinsic graphene behaviour, could be obtained^{204,206}. Using $\text{PbTiO}_3/\text{SrTiO}_3$ superlattices, researchers could tune the transition temperature of the device and minimize adsorbates at the graphene interface, achieving a more ideal coupling²⁰⁷. Despite such advances, the electrostatic coupling between graphene and ferroelectrics is typically reduced compared with what would be expected for a full compensation of the polarization^{203–205}.

The atomistic details and interfacial chemistry governing the interaction and the resulting charge density changes in graphene remained confused until it was demonstrated that the carrier density in graphene can be modulated through coupling to the polarization of an adjacent ferroelectric to create spatially defined potential steps at 180° domain walls, rather than through the fabrication of local gate electrodes²⁰⁸ (FIG. 4c,d). Periodic arrays of p-i junctions (gate tunable to p-n junctions) were realized in air, and density functional theory revealed that at the origin of the potential steps is a complex interplay between polarization, chemistry and defect structures in the device. Now the focus is shifting to the integration of other 2D materials, such as 2D dichalcogenides and topological insulators, on ferroelectrics.

Another area that attracted much interest in the past decade is that of ferroelectric photovoltaics^{209–211}. In conventional photovoltaics, photovoltages are limited by the bandgap of the material. However, in ferroelectric single crystals, photovoltages that are many orders of magnitude higher than the bandgap have been reported. Initial models of this effect — which is called the bulk photovoltaic effect or anomalous photovoltaic effect and

is only observed in non-centrosymmetric materials — described the process as a ‘shift current’; that is, asymmetric quantum scattering in materials²¹² that causes excited carriers to move in a specific direction determined by the polarization. The probability of forming quantum wave packets with the same momentum in opposite directions is not the same for both directions in non-centrosymmetric materials, because the excitation of carriers from one band to another is coupled with their movement from the initial real-space location^{213–215}. The bulk photovoltaic effect explains how materials exhibiting a polarization can give rise to photovoltaic effects without the need for junction-based structures. A second effect is the ballistic photovoltaic effect. The ballistic contribution to the bulk photovoltaic effect is thought to arise from asymmetric scattering from phonons and lattice defects. In polydomain ferroelectrics, the domain walls can act as charge separators, and in ferroelectric heterostructures, a high density of evenly-spaced domain walls can greatly amplify this effect²¹⁶. Strong photoconductivity was observed in BiFeO₃ (REFS 217,218), followed by polarization-direction-dependent photovoltaic and diode behaviour under visible light^{219,220}. In turn, large, above-bandgap photovoltages were reported in domain-structure engineered BiFeO₃ (REF. 221), and efforts were undertaken to understand the bulk-photovoltaic- and domain-wall-based mechanisms^{222–224}. Beyond the work on BiFeO₃ and related systems, one of the most promising developments in recent years has been the design of a new class of low-bandgap polar materials, including [KNbO₃]_{1-x}[BaNi_{1/2}Nb_{1/2}O_{3-δ}]_x, which has a bandgap tunable from 1.1 eV to 3.8 eV and, with $x = 0.1$ and a bandgap of 1.39 eV, exhibits photocurrent densities ~50 times larger than that of classic ferroelectric materials for photovoltaics²²⁵.

The future of ferroelectrics

We have discussed several important developments that have advanced the field of ferroelectric materials over the past decade. To conclude, we survey the most promising directions that the evolution of ferroelectric research might take in the future.

Ferroelectrics and the Materials Genome. Spurred by the development of approaches inspired by the [Materials Genome Initiative](#), there is strong interest in the high-throughput discovery and design of next-generation functional materials^{226,227}. Regular methodological advances that enable the prediction and rapid assessment of complex properties make such work poised to dramatically expand the realm of known or potential functional and ferroelectric materials (FIG. 5a). Crucial for this development will be advances in the high-throughput optimization of descriptors that can be rapidly calculated and mined to identify novel materials, and the exploration of temperature-dependent lattice distortions and phase competition. At the same time, experimentalists will need to keep up with the ever-widening set of candidate materials and will need to develop new methodologies that can reduce the time needed to produce, test and refine materials.

Beyond lattice-mismatch strain. Beyond the approaches previously discussed, a promising route to expand strain control in materials includes the production of free-standing thin-film heterostructures. The concept of on-demand or dynamically tunable strain has the potential to change the way we think about materials. As our ability to produce high-quality materials and integrate them into novel structures improves, we will have the opportunity to produce systems in which strain-induced effects will not be limited to film-substrate lattice mismatch. In particular, micro- and nanoelectromechanical systems based on ferroelectric materials could enable the achievement of unprecedented levels of strain states that vary with time. Such additional control could open the way to new function in devices. To date, there have been only a few studies on free-standing complex oxides, but they are promising, because they demonstrated greatly enhanced piezoelectric coefficients and figures of merit for vibrational energy-harvesting systems²²⁸.

Non-traditional ferroelectrics. Although the vast majority of ferroelectrics are perovskites, the importance of ferroelectric phenomena has triggered a broad search for other materials with switchable polarization. Polymer ferroelectrics have been known for a long time, and in recent years they have shown renewed promise as controllable ferroelectric nanomaterials for optical²²⁹ and electromechanical applications²³⁰. This has inspired a search for small-molecule ferroelectric crystals²³¹. Materials-Genome-type studies have identified a ‘stuffed wurtzite’ structure with hexagonal sheets containing ions that can move out of plane in either direction, yielding a ferroelectric effect²³². Attention has also been focused on ‘hybrid perovskite’ crystals — which have molecular cations on the A site — because of their excellent performance in photovoltaics²³³. However, the nature of the polar order in these materials is unclear. Finally, in 2D transition metal dichalcogenides, electric-field-switchable polar structures have been reported^{234,235}, and there is renewed interest in thiophosphates — the only compounds to show ferroelectricity in van der Waals layered compounds²³⁶. There are also reports of ferroelectric-like behaviour in HfO₂, which can be directly produced on silicon²³⁷.

Real-time studies of ferroelectrics and devices. In recent years, both modelling and characterization methods evolved to provide new levels of understanding across huge time and length scales. In the field of simulations, the community has developed innovative ways to emulate many aspects of *in operando* conditions, including how changes in surface composition, defect concentration, epitaxial strain, interfacial effects and other factors affect the evolution of complex systems. Today it is possible to probe the role of compositional disorder on the temporal- and spatial-dependent dielectric response of very complex relaxor materials and other ferroelectrics using advanced molecular dynamics simulations with extremely large supercells^{19,238–241}. At the same time, new hardware and the development of novel transmission electron microscopy methods (including aberration

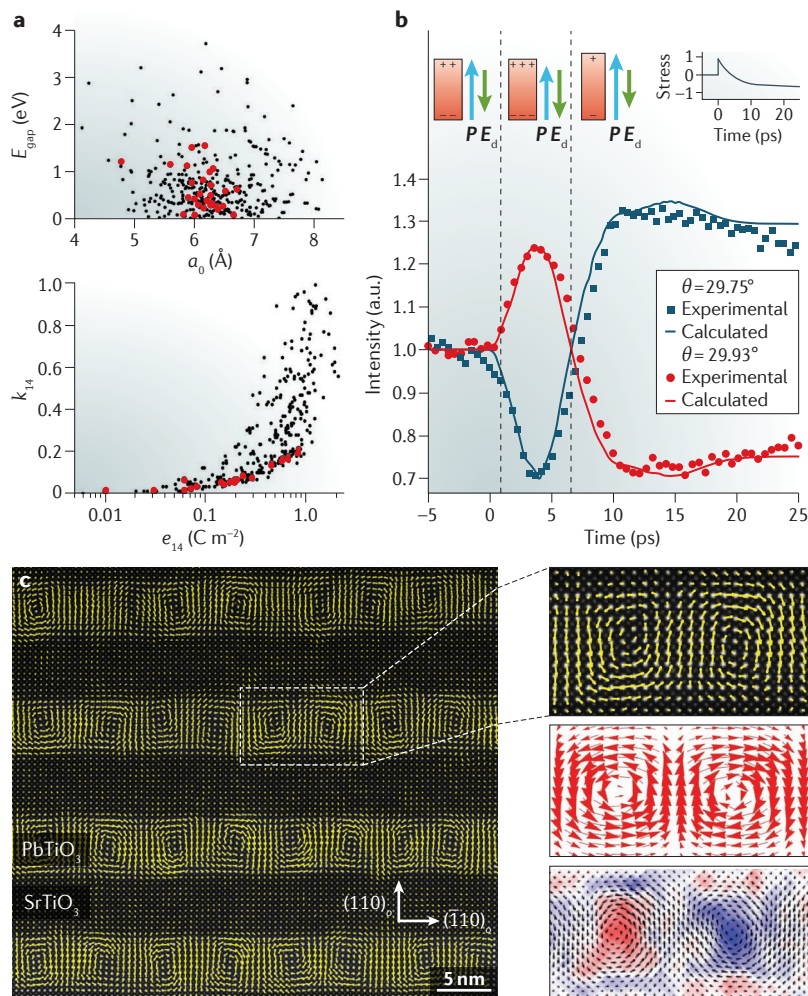


Figure 5 | Promising developments in ferroelectrics research. **a** | High-throughput analysis of advanced piezoelectric materials including the calculated cell parameters (a_0) and their range of bandgaps (E_{gap} ; top), and the electromechanical coupling factor (k_{14}) as a function of the piezoelectric constant (e_{14}) for insulating ABC combinations (bottom). Known combinations are highlighted as filled red circles. **b** | Data and schematic diagrams of the unit-cell response in an ultrafast pump-probe experiment on PbTiO_3 thin films. At $t = 5$ ps, the c lattice parameter reaches a minimum owing to the piezoelectric response to the increase in the depolarization field (\mathbf{E}_d) induced by a bulk photovoltaic shift current. At $t > 10$ ps, carriers have moved to screen the \mathbf{E}_d , driving a long-lived increase in tetragonality. Time scans measured at the indicated angles are fit by modelling the out-of-plane strain of PbTiO_3 as a response to the time-dependent stress profile (shown in the inset). **c** | Observation of vortex–antivortex structures in $\text{PbTiO}_3/\text{SrTiO}_3$ superlattices using cross-sectional atomic-scale imaging with a scanning transmission electron microscope (TEM; the overlaid polarization vector maps represent the locally extracted polar distortion); the subscript ‘o’ refers to orthorhombic indices of the DyScO_3 substrate. A magnified image of a single vortex–antivortex pair: the polarization state within the pair can be visualized easily (top right); phase-field simulations of the same superlattice structure predict the vortex–antivortex pairs (middle right); the curl of polarization ($\nabla \times \mathbf{P}$), for a single vortex pair is extracted from the cross-section TEM polarization vector map (bottom right). a.u., arbitrary units; \mathbf{P} , polarization. Panel **a** is adapted with permission from REF. 270, American Physical Society. Panel **b** is adapted with permission from REF. 255, American Physical Society. Panel **c** is from REF. 267, Nature Publishing Group.

correction and 4D approaches) provide unprecedented atomic-scale insight and are beginning to be able to probe ferroelectrics at the timescales at which real processes, which are important for device operation, happen^{242–245}.

As new systems, better data analysis and big-data approaches spread through the community, it is probable that unprecedented insight on how ferroelectrics work in real systems will be gained. Simply increasing the frame rates and data-acquisition rates during high-resolution imaging may lead to a clearer understanding of ferroelectric switching. Similarly, an advanced scanning-probe microscopy operation mode known as band excitation²⁴⁶ is changing the way ferroelectrics are studied under bias. It enables real-time, *in operando* investigations of ferroelectric switching with nanoscale resolution and with the quantification and extraction of extensive data. In parallel, synchrotron studies and ultrafast probing of ferroelectrics are undergoing a rapid development²⁴⁷. Bright-light sources enable *in operando* studies of devices under applied fields^{248,249}, of the detailed structure of ultrathin films^{250,251}, of the evolution of ferroelectrics under different environmental conditions^{20,252} and, increasingly, ultrafast probing of dynamic responses^{253–256} (FIG. 5b).

Ferroelectrics for energy. Beyond their role in photovoltaics, ferroelectrics are poised to also have an exciting role in heterogeneous catalysis^{257,258}. The polarization of ferroelectrics means that bound charges are present on their surfaces, influencing the surface chemistry in many ways. For example, the electrostatic environment of the surface changes, altering physisorption rates of reactants²⁵⁷, and the bulk polarization can influence the deposition rate and morphology of supported metals²⁵⁸. The polarization also shifts the energy levels of surface atoms, whether they are in a supported metal layer²⁵⁹, in a nonstoichiometric reconstruction²⁶⁰ or in the native oxide²⁶¹. Experimental studies have shown intriguing results, suggesting that ferroelectrics can enhance reactions rates²⁶². An important goal in this field is to combine control of the ferroelectric polarization with the high surface areas required for catalysts.

Topology of ferroelectrics. Although they have been known for a long time, the past few years have seen a strong focus on the study of skyrmions and other topologically protected states in magnetic systems, and on attempts to use them for applications. In a similar way, renewed efforts are concentrated on probing related effects in ferroelectrics²⁶³. In the past decade, theoretical studies have suggested that exotic physical phenomena, including topological structures such as vortices, waves and skyrmions, might arise in ferroelectrics^{264–266}. Some of these proposed structures are finally being observed experimentally²⁶⁷ (FIG. 5c). Despite considerable interest, how to probe, understand, classify and, ultimately, use these topological states of matter in ferroelectrics remains an open question. Similarly, topological insulators, which have different band topologies compared with those of conventional insulators such that interfaces between topological and conventional insulators must always be conductive, are being explored in conjunction with ferroelectrics. The unique characteristics of topological insulators mean that they might have intriguing and synergistic interactions with ferroelectrics, because

ferroelectric nanomaterials require conductive surfaces to compensate their bound charge and reduce the depolarizing field. Recent work²⁶⁸, for example, suggests that under pressure, CsPbI₃ could exhibit a transition to a topological insulating phase and to a switchable ferroelectric phase, and that this ferroelectric topological phase could exhibit an enhanced bulk photovoltaic response²⁶⁹. More work in this area could yield exciting functional materials.

Conclusion

Functional materials, and ferroelectrics in particular, have been an important class of materials both for fundamental research and for applications for the past 70 years. The complex interplay between multiple degrees of freedom in these materials means that

techniques developed to study them have been applied to other condensed matter physics fields with great success (and vice versa). Each year brings new insights and new understanding of these complex materials, as well as new potential applications. In the end, the diverse functionalities of ferroelectrics mean that this complex class of materials will continue to attract interest as their performance in existing devices is improved and novel applications are developed in the years to come. Ultimately, disruptive breakthroughs in high-quality growth, epitaxial nanoscale control and multiscale modelling will provide the ability to create new materials with unprecedented combinations of functional properties. In the long run, the breakthroughs in the field of ferroelectrics will potentially transform society — from energy and medicine, to information and communications.

- Cross, L. E. & Newnham, R. E. In *Ceramics and Civilization III: High Technology Ceramics: Past, Present, and Future* (eds Kingery, W. D. & Lense, E.) 289–305 (American Ceramic Society, 1987).
- de Araujo, C. P., Taylor, G. W. & Scott, J. F. (eds) *Ferroelectric Thin Films: Synthesis and Basic Properties* (Gordon and Breach, 1996).
- Haertling, G. H. Ferroelectric ceramics: history and technology. *J. Am. Ceram. Soc.* **82**, 797–818 (1999).
- Resta, R. Macroscopic polarization in crystalline dielectrics: the geometric phase approach. *Rev. Mod. Phys.* **66**, 899–915 (1994).
- Dawber, M., Rabe, K. M. & Scott, J. F. Physics of thin-film ferroelectric oxides. *Rev. Mod. Phys.* **77**, 1083–1130 (2005).
- Schlom, D. G. *et al.* Strain tuning of ferroelectric thin films. *Annu. Rev. Mater. Res.* **37**, 589–626 (2007).
- Martin, L. W. & Schlom, D. G. Advanced synthesis techniques and routes to new single-phase multiferroics. *Curr. Opin. Sol. State Mater. Sci.* **16**, 199–215 (2012).
- Kalinin, S. V., Borisevich, A. & Fong, D. Beyond condensed matter physics on the nanoscale: the role of ionic and electrochemical phenomena in the physical functionalities of oxide materials. *ACS Nano* **6**, 10423–10437 (2012).
- Cohen, R. E. Origin of ferroelectricity in perovskite oxides. *Nature* **358**, 136–138 (1992).
- Gumbsch, P., Taeri-Baghdarani, S., Brunner, D., Sigle, W. & Ruhle, M. Plasticity and an inverse brittle-to-ductile transition in strontium titanate. *Phys. Rev. Lett.* **87**, 085505 (2001).
- Freund, L. B. & Suresh, S. In *Thin Film Materials: Stress, Defect Formation and Surface Evolution* 60–83, 283–290, 396–416 (Cambridge Univ. Press, 2003).
- Zeches, R. J. *et al.* A strain-driven morphotropic phase boundary in BiFeO₃. *Science* **326**, 977–980 (2009).
- Christen, H. M., Nam, J. H., Kim, H. S., Hatt, A. J. & Spaldin, N. A. Stress-induced *R*-*M_xM_{1-x}T* symmetry changes in BiFeO₃ films. *Phys. Rev. B* **83**, 144107 (2011).
- Junquera, J. & Ghosez, P. Critical thickness for ferroelectricity in perovskite ultrathin films. *Nature* **422**, 506–509 (2003).
- Fong, D. D. *et al.* Ferroelectricity in ultrathin perovskite films. *Science* **304**, 1650–1653 (2004).
- Sai, N., Kolpak, A. M. & Rappe, A. M. Ferroelectricity in ultrathin perovskite films. *Phys. Rev. B* **72**, 020101 (2005).
- Kolpak, A. M., Sai, N. & Rappe, A. M. Short-circuit boundary conditions in ferroelectric PbTiO₃ thin films. *Phys. Rev. B* **74**, 054112 (2006).
- Jia, C. L. *et al.* Unit-cell scale mapping of ferroelectricity and tetragonality in epitaxial ultrathin ferroelectric films. *Nat. Mater.* **6**, 64–69 (2007).
- Spanier, J. E. *et al.* Ferroelectric phase transition in individual single-crystalline BaTiO₃ nanowires. *Nano Lett.* **6**, 735–739 (2006).
- Wang, R. V. *et al.* Reversible chemical switching of a ferroelectric film. *Phys. Rev. Lett.* **102**, 047601 (2009).
- Stengel, M., Vanderbilt, D. & Spaldin, N. A. Enhancement of ferroelectricity at metal-oxide interfaces. *Nat. Mater.* **8**, 392–397 (2009).
- Neaton, J. B. & Rabe, K. M. Theory of polarization enhancement in epitaxial BaTiO₃/SrTiO₃ superlattices. *Appl. Phys. Lett.* **82**, 1586–1588 (2003).
- Sai, N., Meyer, B. & Vanderbilt, D. Compositional inversion symmetry breaking in ferroelectric perovskites. *Phys. Rev. Lett.* **84**, 5636–5639 (2000).
- Nakhmanson, S. M., Rabe, K. M. & Vanderbilt, D. Polarization enhancement in two- and three-component ferroelectric superlattices. *Appl. Phys. Lett.* **87**, 102906 (2005).
- Nakhmanson, S. M., Rabe, K. M. & Vanderbilt, D. Predicting polarization enhancement in multicomponent ferroelectric superlattices. *Phys. Rev. B* **73**, 060101 (2006).
- Corbett, M. H., Bowman, R. M., Gregg, J. M. & Foord, D. T. Enhancement of dielectric constant and associated coupling of polarization behavior in thin film relaxor superlattices. *Appl. Phys. Lett.* **79**, 815–817 (2001).
- Shimuta, T. *et al.* Enhancement of remanent polarization in epitaxial BaTiO₃/SrTiO₃ superlattices with “asymmetric” structure. *J. Appl. Phys.* **91**, 2290–2294 (2002).
- Warusawithana, M. P., Colla, E. V., Eckstein, J. N. & Weissman, M. B. Artificial dielectric superlattices with broken inversion symmetry. *Phys. Rev. Lett.* **90**, 036802 (2003).
- Kim, L., Jung, D., Kim, J., Kim, Y. S. & Lee, J. Strain manipulation in BaTiO₃/SrTiO₃ artificial lattice toward high dielectric constant and its nonlinearity. *Appl. Phys. Lett.* **82**, 2118–2120 (2003).
- Christen, H. M., Specht, E. D., Silliman, S. S. & Harshavardhan, K. S. Ferroelectric and antiferroelectric coupling in superlattices of paraelectric perovskites at room temperature. *Phys. Rev. B* **68**, 020101 (2003).
- Tian, W. *et al.* Structural evidence for enhanced polarization in a commensurate short-period BaTiO₃/SrTiO₃ superlattice. *Appl. Phys. Lett.* **89**, 092905 (2006).
- Tenne, D. A. *et al.* Probing nanoscale ferroelectricity by ultraviolet raman spectroscopy. *Science* **313**, 1614–1616 (2006).
- Lee, H. N., Christen, H. M., Chisholm, M. F., Rouleau, C. M. & Lowndes, D. H. Strong polarization enhancement in asymmetric three-component ferroelectric superlattices. *Nature* **433**, 395–399 (2005).
- Dawber, M. *et al.* Unusual behavior of the ferroelectric polarization in PbTiO₃/SrTiO₃ superlattices. *Phys. Rev. Lett.* **95**, 177601 (2005).
- Bousquet, E. *et al.* Improper ferroelectricity in perovskite oxide artificial superlattices. *Nature* **452**, 732–736 (2008).
- Haeni, J. H. *et al.* Room-temperature ferroelectricity in strained SrTiO₃. *Nature* **430**, 758–761 (2004).
- Choi, K. J. *et al.* Enhancement of ferroelectricity in strained BaTiO₃ thin films. *Science* **306**, 1005–1009 (2004).
- Holcomb, M. B. *et al.* Probing the evolution of antiferromagnetism in multiferroics. *Phys. Rev. B* **81**, 134406 (2010).
- Sando, D. *et al.* Crafting the magnonic and spintronic response of BiFeO₃ films by epitaxial strain. *Nat. Mater.* **12**, 641–646 (2013).
- Ederer, C. & Spaldin, N. Effect of epitaxial strain on the spontaneous polarization of thin film ferroelectrics. *Phys. Rev. Lett.* **95**, 257601 (2005).
- Ravindran, P., Vidy, R., Kjekshus, A., Fjellvåg, H. & Eriksson, O. Theoretical investigation of magnetoelectric behavior in BiFeO₃. *Phys. Rev. B* **74**, 224412 (2006).
- Bea, H. *et al.* Evidence for room-temperature multiferroicity in a compound with a giant axial ratio. *Phys. Rev. Lett.* **102**, 217603 (2009).
- Ricinschi, D., Yun, K. Y. & Okuyama, M. A mechanism for the 150 μC cm⁻² polarization of BiFeO₃ films based on first-principles calculations and new structural data. *J. Phys. Condens. Matter* **18**, L97–L105 (2006).
- Damodaran, A., Lee, S., Karthik, J., MacLaren, S. & Martin, L. Temperature and thickness evolution and epitaxial breakdown in highly strained BiFeO₃ thin films. *Phys. Rev. B* **85**, 024113 (2012).
- Damodaran, A. R., Breckenfeld, E., Choquette, A. K. & Martin, L. W. Stabilization of mixed-phase structures in highly strained BiFeO₃ thin films via chemical-alloying. *Appl. Phys. Lett.* **100**, 082904 (2012).
- Ouyang, J., Zhang, W., Huang, X. & Roytburd, A. L. Thermodynamics of formation of tetragonal and rhombohedral heterophase polydomains in epitaxial ferroelectric thin films. *Acta Mater.* **59**, 3779–3791 (2011).
- Zhang, J. X. *et al.* Large field-induced strains in a lead-free piezoelectric material. *Nat. Nanotechnol.* **6**, 98–102 (2011).
- Vasudevan, R. K. *et al.* Nanoscale control of phase variants in strain-engineered BiFeO₃. *Nano Lett.* **11**, 3346–3354 (2011).
- Damodaran, A. R. *et al.* Nanoscale structure and mechanism for enhanced electromechanical response of highly strained BiFeO₃ thin films. *Adv. Mater.* **23**, 3170–3175 (2011).
- Martin, L. W. *et al.* Growth and structure of PbVO₃ thin films. *Appl. Phys. Lett.* **90**, 062903 (2007).
- Kumar, A. *et al.* Polar and magnetic properties of PbVO₃ thin films. *Phys. Rev. B* **75**, 060101 (2007).
- Lee, J. H. *et al.* A strong ferroelectric ferromagnet created by means of spin-lattice coupling. *Nature* **466**, 954–958 (2010).
- Shin, Y.-H., Grinberg, I., Chen, I.-W. & Rappe, A. M. Nucleation and growth mechanism of ferroelectric domain-wall motion. *Nature* **449**, 881–884 (2007).
- Liu, S., Grinberg, I. & Rappe, A. M. Intrinsic ferroelectric switching from first principles. *Nature* **534**, 360–363 (2016).
- Ganpule, C. S. *et al.* Imaging three-dimensional polarization in epitaxial polydomain ferroelectric thin films. *J. Appl. Phys.* **91**, 1477–1481 (2002).
- Koukhar, V., Pertsev, N. & Waser, R. Thermodynamic theory of epitaxial ferroelectric thin films with dense domain structures. *Phys. Rev. B* **64**, 214103 (2001).

57. Li, Y. L., Hu, S. Y. & Chen, L. Q. Ferroelectric domain morphologies of (001) $\text{PbZr}_{1-x}\text{Ti}_x\text{O}_3$ epitaxial thin films. *J. Appl. Phys.* **97**, 034112 (2005).
58. Kukhar, V., Pertsev, N., Kohlstedt, H. & Waser, R. Polarization states of polydomain epitaxial $\text{Pb}(\text{Zr}_{1-x}\text{Ti}_x)\text{O}_3$ thin films and their dielectric properties. *Phys. Rev. B* **73**, 214103 (2006).
59. Karthik, J. & Martin, L. Pyroelectric properties of polydomain epitaxial $\text{Pb}(\text{Zr}_{1-x}\text{Ti}_x)\text{O}_3$ thin films. *Phys. Rev. B* **84**, 024102 (2011).
60. Karthik, J. & Martin, L. W. Effect of domain walls on the electrocaloric properties of $\text{Pb}(\text{Zr}_{1-x}\text{Ti}_x)\text{O}_3$ thin films. *Appl. Phys. Lett.* **99**, 032904 (2011).
61. Karthik, J., Damodaran, A. & Martin, L. Effect of 90° domain walls on the low-field permittivity of $\text{PbZr}_{0.2}\text{Ti}_{0.8}\text{O}_3$ thin films. *Phys. Rev. Lett.* **108**, 167601 (2012).
62. Karthik, J., Agar, J. C., Damodaran, A. R. & Martin, L. W. Effect of 90 degrees domain walls and thermal expansion mismatch on the pyroelectric properties of epitaxial $\text{PbZr}_{0.2}\text{Ti}_{0.8}\text{O}_3$ thin films. *Phys. Rev. Lett.* **109**, 257602 (2012).
63. Karthik, J., Damodaran, A. R. & Martin, L. W. Epitaxial ferroelectric heterostructures fabricated by selective area epitaxy of SrRuO_3 using an MgO mask. *Adv. Mater.* **24**, 1610–1615 (2012).
64. Chu, Y. H. *et al.* Nanoscale domain control in multiferroic BiFeO_3 thin films. *Adv. Mater.* **18**, 2307–2311 (2006).
65. Pabst, G. W., Martin, L. W., Chu, Y. & Ramesh, R. Leakage mechanisms in BiFeO_3 thin films. *Appl. Phys. Lett.* **90**, 072902 (2007).
66. Folkman, C. M. *et al.* Stripe domain structure in epitaxial (001) BiFeO_3 thin films on orthorhombic TbScO_3 substrate. *Appl. Phys. Lett.* **94**, 251911 (2009).
67. Chen, Z. *et al.* 180° ferroelectric stripe nanodomains in BiFeO_3 thin films. *Nano. Lett.* **15**, 6506–6513 (2015).
68. Chu, Y. H. *et al.* Domain control in multiferroic BiFeO_3 through substrate vicinity. *Adv. Mater.* **19**, 2662–2666 (2007).
69. Chen, Y. B. *et al.* Ferroelectric domain structures of epitaxial (001) BiFeO_3 thin films. *Appl. Phys. Lett.* **90**, 072907 (2007).
70. Jang, H. W. *et al.* Domain engineering for enhanced ferroelectric properties of epitaxial (001) BiFeO_3 thin films. *Adv. Mater.* **21**, 817–825 (2009).
71. Chu, Y. *et al.* Nanoscale control of domain architectures in BiFeO_3 thin films. *Nano Lett.* **9**, 1726–1730 (2009).
72. Park, J. W. *et al.* Origin of suppressed polarization in BiFeO_3 films. *Appl. Phys. Lett.* **97**, 212904 (2010).
73. Baek, S. *et al.* The nature of polarization fatigue in BiFeO_3 . *Adv. Mater.* **23**, 1621–1625 (2011).
74. Baek, S. H. *et al.* Ferroelastic switching for nanoscale non-volatile magnetoelectric devices. *Nat. Mater.* **9**, 309–314 (2010).
75. Giенcke, J. E., Folkman, C. M., Baek, S. & Eom, C. Tailoring the domain structure of epitaxial BiFeO_3 thin films. *Curr. Opin. Sol. State Mater. Sci.* **18**, 39–45 (2014).
76. Zhang, J., Weiss, C. V. & Alpay, S. P. Effect of thermal stresses on the dielectric properties of strontium titanate thin films. *Appl. Phys. Lett.* **99**, 042902 (2011).
77. Zembilgotov, A. G., Pertsev, N. A., Böttger, U. & Waser, R. Effect of anisotropic in-plane strains on phase states and dielectric properties of epitaxial ferroelectric thin films. *Appl. Phys. Lett.* **86**, 052903 (2005).
78. Biegalski, M. D. *et al.* Influence of anisotropic strain on the dielectric and ferroelectric properties of SrTiO_3 thin films on DyScO_3 substrates. *Phys. Rev. B* **79**, 224117 (2009).
79. Harrington, S. A. *et al.* Thick lead-free ferroelectric films with high curie temperatures through nanocomposite-induced strain. *Nat. Nanotechnol.* **6**, 491–495 (2011).
80. Cheng, C.-J., Borisevich, A. Y., Kan, D., Takeuchi, I. & Nagarajan, V. Nanoscale structural and chemical properties of antipolar clusters in *sm*-doped BiFeO_3 ferroelectric epitaxial thin films. *Chem. Mater.* **22**, 2588–2596 (2010).
81. Cheng, C.-J., Kan, D., Anbusathaiah, V., Takeuchi, I. & Nagarajan, V. Microstructure-electromechanical property correlations in rare-earth substituted BiFeO_3 epitaxial thin films at morphotopic phase boundaries. *Appl. Phys. Lett.* **97**, 212905 (2010).
82. Kan, D., Anbusathaiah, V. & Takeuchi, I. Chemical substitution-induced ferroelectric polarization rotation in BiFeO_3 . *Adv. Mater.* **23**, 1765–1769 (2011).
83. Borisevich, A. Y. *et al.* Atomic-scale evolution of modulated phases at the ferroelectric-antiferroelectric morphotropic phase boundary controlled by flexoelectric interaction. *Nat. Commun.* **3**, 775 (2012).
84. Kan, D., Cheng, C., Nagarajan, V. & Takeuchi, I. in *Functional Metal Oxides* (eds Ogale, S. B., Venkatesan, T. V. & Blamire, M. G.) 195–219 (Wiley-VCH, 2013).
85. Breckenfeld, E. *et al.* Effect of growth induced (non)stoichiometry on the structure, dielectric response, and thermal conductivity of SrTiO_3 thin films. *Chem. Mater.* **24**, 331–337 (2012).
86. Breckenfeld, E., Wilson, R. B. & Martin, L. W. Effect of growth induced (non)stoichiometry on the thermal conductivity, permittivity, and dielectric loss of LaAlO_3 films. *Appl. Phys. Lett.* **103**, 082901 (2013).
87. Breckenfeld, E. *et al.* Effect of growth induced (non) stoichiometry on interfacial conductance in $\text{LaAlO}_3/\text{SrTiO}_3$. *Phys. Rev. Lett.* **110**, 196804 (2013).
88. Breckenfeld, E., Shah, A. B. & Martin, L. W. Strain evolution in non-stoichiometric heteroepitaxial thin-film perovskites. *J. Mater. Chem. C* **1**, 8052–8059 (2013).
89. Lee, C.-H. *et al.* Exploiting dimensionality and defect mitigation to create tunable microwave dielectrics. *Nature* **502**, 532–536 (2013).
90. Breckenfeld, E., Bronn, N., Mason, N. & Martin, L. W. Tunability of conduction at the $\text{LaAlO}_3/\text{SrTiO}_3$ heterointerface: thickness and compositional studies. *Appl. Phys. Lett.* **105**, 121610 (2014).
91. Breckenfeld, E., Chen, Z., Damodaran, A. R. & Martin, L. W. Effects of nonequilibrium growth, nonstoichiometry, and film orientation on the metal-to-insulator transition in NdNiO_3 thin films. *ACS Appl. Mater. Interfaces* **6**, 22436–22444 (2014).
92. Damodaran, A. R., Breckenfeld, E., Chen, Z., Lee, S. & Martin, L. W. Enhancement of ferroelectric curie temperature in BaTiO_3 films via strain-induced defect dipole alignment. *Adv. Mater.* **26**, 6341–6347 (2014).
93. Xu, R., Karthik, J., Damodaran, A. R. & Martin, L. W. Stationary domain wall contribution to enhanced ferroelectric susceptibility. *Nat. Commun.* **5**, 3120 (2014).
94. Xu, R. *et al.* Ferroelectric polarization reversal via successive ferroelastic transitions. *Nat. Mater.* **14**, 79–86 (2015).
95. Xu, R., Zhang, J., Chen, Z. & Martin, L. W. Orientation-dependent structural phase diagrams and dielectric properties of $\text{PbZr}_{1-x}\text{Ti}_x\text{O}_3$ polydomain thin films. *Phys. Rev. B* **91**, 144106 (2015).
96. Daniels, J. E. *et al.* Neutron diffraction study of the polarization reversal mechanism in [111]_c-oriented $\text{Pb}(\text{Zn}_{1-x}\text{Nb}_x)\text{O}_3$ - $x\text{PbTiO}_3$. *J. Appl. Phys.* **101**, 104108 (2007).
97. Daniels, J. E. *et al.* Two-step polarization reversal in biased ferroelectrics. *J. Appl. Phys.* **115**, 224104 (2014).
98. Benedek, N. A. & Fennie, C. J. Hybrid improper ferroelectricity: a mechanism for controllable polarization-magnetization coupling. *Phys. Rev. Lett.* **106**, 107204 (2011).
99. Rondinelli, J. M. & Fennie, C. J. Octahedral rotation-induced ferroelectricity in cation ordered perovskites. *Adv. Mater.* **24**, 1961–1968 (2012).
100. Mulder, A. T., Benedek, N. A., Rondinelli, J. M. & Fennie, C. J. Turning ABO_3 antiferroelectrics into ferroelectrics: design rules for practical rotation-driven ferroelectricity in double perovskites and $\text{A}_2\text{B}_2\text{O}_7$ ruddlesden-popper compounds. *Adv. Funct. Mater.* **23**, 4810–4820 (2013).
101. Yu, P. *et al.* Interface control of bulk ferroelectric polarization. *Proc. Nat. Acad. Sci. USA* **109**, 9710–9715 (2012).
102. Spurgeon, S. R. *et al.* Thickness-dependent crossover from charge- to strain-mediated magnetoelectric coupling in ferromagnetic/piezoelectric oxide heterostructures. *ACS Nano* **8**, 894–903 (2014).
103. Spurgeon, S. R. *et al.* Polarization screening-induced magnetic phase gradients at complex oxide interfaces. *Nat. Commun.* **6**, 6735 (2015).
104. Borisevich, A. *et al.* Suppression of octahedral tilts and associated changes in electronic properties at epitaxial oxide heterostructure interfaces. *Phys. Rev. Lett.* **105**, 087204 (2010).
105. Kim, Y. *et al.* Interplay of octahedral tilts and polar order in BiFeO_3 films. *Adv. Mater.* **25**, 2497–2504 (2013).
106. Chen, Z. H., Damodaran, A. R., Xu, R., Lee, S. & Martin, L. W. Effect of “symmetry mismatch” on the domain structure of rhombohedral BiFeO_3 thin films. *Appl. Phys. Lett.* **104**, 182908 (2014).
107. Zubko, P., Catalan, G. & Tagantsev, A. K. Flexoelectric effect in solids. *Annu. Rev. Mater. Res.* **43**, 387–421 (2013).
108. Yudin, P. V. & Tagantsev, A. K. Fundamentals of flexoelectricity in solids. *Nanotechnology* **24**, 432001 (2013).
109. Resta, R. Towards a bulk theory of flexoelectricity. *Phys. Rev. Lett.* **105**, 127601 (2010).
110. Hong, J. & Vanderbilt, D. First-principles theory of frozen-in flexoelectricity. *Phys. Rev. B* **84**, 180101 (2011).
111. Stengel, M. Flexoelectricity from density-functional perturbation theory. *Phys. Rev. B* **88**, 174106 (2013).
112. Biancoli, A., Fancher, C. M., Jones, J. L. & Damjanovic, D. Breaking of macroscopic centric symmetry in paraelectric phases of ferroelectric materials and implications for flexoelectricity. *Nat. Mater.* **14**, 224–229 (2015).
113. Catalan, G., Sinnamon, L. J. & Gregg, J. M. The effect of flexoelectricity on the dielectric properties of inhomogeneously strained ferroelectric thin films. *J. Phys. Condens. Matter* **16**, 2253 (2004).
114. Catalan, G., Noheda, B., McAneney, J., Sinnamon, L. J. & Gregg, J. M. Strain gradients in epitaxial ferroelectrics. *Phys. Rev. B* **72**, 020102 (2005).
115. Lu, H. *et al.* Mechanical writing of ferroelectric polarization. *Science* **336**, 59–61 (2012).
116. Lee, D. *et al.* Giant flexoelectric effect in ferroelectric epitaxial thin films. *Phys. Rev. Lett.* **107**, 057602 (2011).
117. Catalan, G. *et al.* Flexoelectric rotation of polarization in ferroelectric thin films. *Nat. Mater.* **10**, 963–967 (2011).
118. Lee, D. *et al.* Flexoelectric control of defect formation in ferroelectric epitaxial thin films. *Adv. Mater.* **26**, 5005–5011 (2014).
119. Mangalam, R. V. K., Karthik, J., Damodaran, A. R., Agar, J. C. & Martin, L. W. Unexpected crystal and domain structures and properties in compositionally graded $\text{PbZr}_{1-x}\text{Ti}_x\text{O}_3$ thin films. *Adv. Mater.* **25**, 1761–1767 (2013).
120. Mangalam, R. V. K., Agar, J. C., Damodaran, A. R., Karthik, J. & Martin, L. W. Improved pyroelectric figures of merit in compositionally graded $\text{PbZr}_{1-x}\text{Ti}_x\text{O}_3$ thin films. *ACS Appl. Mater. Interfaces* **5**, 13235–13241 (2013).
121. Agar, J. C. *et al.* Complex evolution of built-in potential in compositionally-graded $\text{PbZr}_{1-x}\text{Ti}_x\text{O}_3$ thin films. *ACS Nano* **9**, 7332–7342 (2015).
122. Karthik, J., Mangalam, R. V. K., Agar, J. C. & Martin, L. W. Large built-in electric fields due to flexoelectricity in compositionally graded ferroelectric thin films. *Phys. Rev. B* **87**, 024111 (2013).
123. Bhaskar, U. K. *et al.* A flexoelectric microelectromechanical system on silicon. *Nat. Nanotechnol.* **11**, 263–266 (2016).
124. Scott, J. F. Electrocaloric materials. *Annu. Rev. Mater. Res.* **41**, 229–240 (2011).
125. Valant, M. Electrocaloric materials for future solid-state refrigeration technologies. *Prog. Mater. Sci.* **57**, 980–1009 (2012).
126. Alpay, S. P., Mantese, J., Trolier-McKinstry, S., Zhang, Q. & Whatmore, R. W. Next-generation electrocaloric and pyroelectric materials for solid-state electrothermal energy interconversion. *MRS Bull.* **39**, 1099–1111 (2014).
127. Moya, X., Kar-Narayan, S. & Mathur, N. D. Caloric materials near ferroic phase transitions. *Nat. Mater.* **13**, 439–450 (2014).
128. Mischenko, A. S., Zhang, Q., Scott, J. F., Whatmore, R. W. & Mathur, N. D. Giant electrocaloric effect in thin-film $\text{PbZr}_{0.95}\text{Ti}_{0.05}\text{O}_3$. *Science* **311**, 1270–1271 (2006).
129. Mischenko, A. S., Zhang, Q., Whatmore, R. W., Scott, J. F. & Mathur, N. D. Giant electrocaloric effect in the thin film relaxor ferroelectric $0.9\text{PbMg}_{0.1}\text{Nb}_{0.9}\text{O}_3$ - 0.1PbTiO_3 near room temperature. *Appl. Phys. Lett.* **89**, 242912 (2006).
130. Correia, T. M. *et al.* Investigation of the electrocaloric effect in a $\text{PbMg}_{0.2}\text{Nb}_{0.8}\text{O}_3$ - PbTiO_3 relaxor thin film. *Appl. Phys. Lett.* **95**, 182904 (2009).
131. Chen, H., Ren, T., Wu, X., Yang, Y. & Liu, L. Giant electrocaloric effect in lead-free thin film of strontium bismuth tantalate. *Appl. Phys. Lett.* **94**, 182902 (2009).
132. Akcay, G., Alpay, S. P., Mantese, J. V. & Rossetti, G. A. Magnitude of the intrinsic electrocaloric effect in ferroelectric perovskite thin films at high electric fields. *Appl. Phys. Lett.* **90**, 252909 (2007).

133. Marathe, M. & Ederer, C. Electrocaloric effect in BaTiO₃: a first-principles-based study on the effect of misfit strain. *Appl. Phys. Lett.* **104**, 212902 (2014).
134. Liu, Y., Infante, I. C., Lou, X., Lupascu, D. C. & Dkhil, B. Giant mechanically-mediated electrocaloric effect in ultrathin ferroelectric capacitors at room temperature. *Appl. Phys. Lett.* **104**, 012907 (2014).
135. Zhang, J., Cole, M. W. & Alpay, S. P. Pyroelectric properties of barium strontium titanate films: effect of thermal stresses. *J. Appl. Phys.* **108**, 054103 (2010).
136. Zhang, J., Alpay, S. P. & Rossetti, G. A. Influence of thermal stresses on the electrocaloric properties of ferroelectric films. *Appl. Phys. Lett.* **98**, 132907 (2011).
137. Zhang, J., Xu, R., Damodaran, A. R., Chen, Z.-H. & Martin, L. W. Understanding order in compositionally graded ferroelectrics: flexoelectricity, gradient, and depolarization field effects. *Phys. Rev. B* **89**, 224101 (2014).
138. Kesim, M. T., Zhang, J., Alpay, S. P. & Martin, L. W. Enhanced electrocaloric and pyroelectric response from ferroelectric multilayers. *Appl. Phys. Lett.* **105**, 052901 (2014).
139. Espinal, Y. *et al.* Pyroelectric and dielectric properties of ferroelectric films with interposed dielectric buffer layers. *Appl. Phys. Lett.* **105**, 232905 (2014).
140. Peng, B., Fan, H. & Zhang, Q. A giant electrocaloric effect in nanoscale antiferroelectric and ferroelectric phases coexisting in a relaxor Pb_{0.8}Ba_{0.2}ZrO₃ thin film at room temperature. *Adv. Funct. Mater.* **23**, 2987–2992 (2013).
141. Pirc, R., Rožič, B., Koruza, J., Malič, B. & Kutnjak, Z. Negative electrocaloric effect in antiferroelectric PbZrO₃. *Europhys. Lett.* **107**, 17002 (2014).
142. Geng, W. *et al.* Giant negative electrocaloric effect in antiferroelectric La-doped Pb(ZrTi)O₃ thin films near room temperature. *Adv. Mater.* **27**, 3165–3169 (2015).
143. Moya, X. *et al.* Giant electrocaloric strength in single-crystal BaTiO₃. *Adv. Mater.* **25**, 1360–1365 (2013).
144. Moya, X. *et al.* Giant and reversible extrinsic magnetocaloric effects in La_{0.3}Ca_{0.6}MnO₃ films due to strain. *Nat. Mater.* **12**, 52–58 (2013).
145. Fletcher, P. C., Mangalam, V. K. R., Martin, L. W. & King, W. P. Field emission from nanometer-scale tips of crystalline PbZr_{1-x}Ti_xO₃. *J. Vac. Sci. Technol. B* **31**, 021805 (2013).
146. Fletcher, P. C., Mangalam, V. K. R., Martin, L. W. & King, W. P. Pyroelectric electron emission from nanometer-thick films of PbZr_{1-x}Ti_xO₃. *Appl. Phys. Lett.* **102**, 192908 (2013).
147. Bhatia, B., Damodaran, A. R., Cho, H., Martin, L. W. & King, W. P. High-frequency thermal-electrical cycles for pyroelectric energy conversion. *J. Appl. Phys.* **116**, 194509 (2014).
148. Lu, S. G. *et al.* Comparison of directly and indirectly measured electrocaloric effect in relaxor ferroelectric polymers. *Appl. Phys. Lett.* **97**, 202901 (2010).
149. Tong, T., Karthik, J., Mangalam, R. V. K., Martin, L. W. & Cahill, D. G. Reduction of the electrocaloric entropy change of ferroelectric PbZr_{1-x}Ti_xO₃ epitaxial layers due to an elastocaloric effect. *Phys. Rev. B* **90**, 094116 (2014).
150. Goupil, F. L., Berenov, A., Axelsson, A., Valant, M. & Alford, N. M. Direct and indirect electrocaloric measurements on (001)-70PbMg_{1/3}Nb_{2/3}O₃-30PbTiO₃ single crystals. *J. Appl. Phys.* **111**, 124109 (2012).
151. Bhatia, B. *et al.* Pyroelectric current measurements on PbZr_{0.2}Ti_{0.8}O₃ epitaxial layers. *J. Appl. Phys.* **112**, 104106 (2012).
152. Botea, M., Iuga, A. & Ptilinie, L. Giant pyroelectric coefficient determined from the frequency dependence of the pyroelectric signal generated by epitaxial Pb(Zr_{0.2}Ti_{0.8})O₃ layers grown on single crystal SrTiO₃ substrates. *Appl. Phys. Lett.* **103**, 232902 (2013).
153. Tong, T., Karthik, J., Martin, L. W. & Cahill, D. G. Secondary effects in wide frequency range measurements of the pyroelectric coefficient of Ba_{0.6}Sr_{0.4}TiO₃ and PbZr_{0.2}Ti_{0.8}O₃ epitaxial layers. *Phys. Rev. B* **90**, 155423 (2014).
154. Kolodiazny, T. *et al.* Thermoelectric power, hall effect, and mobility of *n*-type BaTiO₃. *Phys. Rev. B* **68**, 085205 (2003).
155. Kolodiazny, T. Insulator-metal transition and anomalous sign reversal of the dominant charge carriers in perovskite BaTiO_{3-δ}. *Phys. Rev. B* **78**, 045107 (2008).
156. Lee, S., Yang, G., Wilke, R. H. T., Trolrier-McKinstry, S. & Randall, C. A. Thermopower in highly reduced *n*-type ferroelectric and related perovskite oxides and the role of heterogeneous nonstoichiometry. *Phys. Rev. B* **79**, 134110 (2009).
157. Lee, S., Wilke, R. H. T., Trolrier-McKinstry, S., Zhang, S. & Randall, C. A. Sr_{1-x}Ba_xNb₂O_{6-δ} ferroelectric-thermoelectrics: crystal anisotropy, conduction mechanism, and power factor. *Appl. Phys. Lett.* **96**, 031910 (2010).
158. Lee, S., Dursun, S., Duran, C. & Randall, C. A. Thermoelectric power factor enhancement of textured ferroelectric Sr_{1-x}Ba_xNb₂O_{6-δ} ceramics. *J. Mater. Res.* **26**, 26–30 (2011).
159. Lee, S., Bock, J. A., Trolrier-McKinstry, S. & Randall, C. A. Ferroelectric-thermoelectricity and mot transition of ferroelectric oxides with high electronic conductivity. *J. Eur. Ceram. Soc.* **32**, 3971–3988 (2012).
160. Bock, J. A., Trolrier-McKinstry, S., Mahan, G. D. & Randall, C. A. Polarization-based perturbations to thermopower and electronic conductivity in highly conductive tungsten bronze structured (Sr, Ba)Nb₂O₆: relaxors versus normal ferroelectrics. *Phys. Rev. B* **90**, 115106 (2014).
161. Hopkins, P. E. *et al.* Effects of coherent ferroelastic domain walls on the thermal conductivity and Kapitza conductance in bismuth ferrite. *Appl. Phys. Lett.* **102**, 121903 (2013).
162. Ihlefeld, J. F. *et al.* Room-temperature voltage tunable phonon thermal conductivity via reconfigurable interfaces in ferroelectric thin films. *Nano Lett.* **15**, 1791–1795 (2015).
163. Catalan, G., Seidel, J., Ramesh, R. & Scott, J. F. Domain wall nanoelectronics. *Rev. Mod. Phys.* **84**, 119–156 (2012).
164. Vasudevan, R. K. *et al.* Domain wall conduction and polarization-mediated transport in ferroelectrics. *Adv. Funct. Mater.* **23**, 2592–2616 (2013).
165. Seidel, J. *et al.* Conduction at domain walls in oxide multiferroics. *Nat. Mater.* **8**, 229–234 (2009).
166. Eliseev, E. A., Morozovska, A. N., Svecnikov, G. S., Gopalan, V. & Shur, V. Y. Static conductivity of charged domain walls in uniaxial ferroelectric semiconductors. *Phys. Rev. B* **83**, 235313 (2011).
167. Eliseev, E. A., Morozovska, A. N., Svecnikov, G. S., Maksymovych, P. & Kalinin, S. V. Domain wall conduction in multiaxial ferroelectrics. *Phys. Rev. B* **85**, 045312 (2012).
168. Morozovska, A. N., Vasudevan, R. K., Maksymovych, P., Kalinin, S. V. & Eliseev, E. A. Anisotropic conductivity of uncharged domain walls in BiFeO₃. *Phys. Rev. B* **86**, 085315 (2012).
169. Farokhipoor, S. & Noheda, B. Conduction through 71° domain walls in BiFeO₃ thin films. *Phys. Rev. Lett.* **107**, 127601 (2011).
170. Guyonnet, J., Gaponenko, I., Gariglio, S. & Paruch, P. Conduction at domain walls in insulating Pb(Zr_{0.2}Ti_{0.8})O₃ thin films. *Adv. Mater.* **23**, 5377–5382 (2011).
171. Sluka, T., Tagantsev, A. K., Bednyakov, P. & Setter, N. Free-electron gas at charged domain walls in insulating BaTiO₃. *Nat. Commun.* **4**, 1808 (2013).
172. Meier, D. *et al.* Anisotropic conductance at improper ferroelectric domain walls. *Nat. Mater.* **11**, 284–288 (2012).
173. Wu, W., Horibe, Y., Lee, N., Cheong, S.-W. & Grest, J. R. Conduction of topologically protected charged ferroelectric domain walls. *Phys. Rev. Lett.* **108**, 077203 (2012).
174. Schröder, M. *et al.* Conducting domain walls in lithium niobate single crystals. *Adv. Funct. Mater.* **22**, 3936–3944 (2012).
175. Gaponenko, I., Tückmantel, P., Karthik, J., Martin, L. W. & Paruch, P. Towards reversible control of domain wall conduction in Pb(Zr_{0.2}Ti_{0.8})O₃ thin films. *Appl. Phys. Lett.* **106**, 162902 (2015).
176. Seidel, J. *et al.* Domain wall conductivity in La-doped BiFeO₃. *Phys. Rev. Lett.* **105**, 197603 (2010).
177. Vasudevan, R. K. *et al.* Domain wall geometry controls conduction in ferroelectrics. *Nano Lett.* **12**, 5524–5531 (2012).
178. He, Q. *et al.* Magnetotransport at domain walls in BiFeO₃. *Phys. Rev. Lett.* **108**, 067203 (2012).
179. Balke, N. *et al.* Enhanced electric conductivity at ferroelectric vortex cores in BiFeO₃. *Nat. Phys.* **8**, 81–88 (2012).
180. Maksymovych, P. *et al.* Dynamic conductivity of ferroelectric domain walls in BiFeO₃. *Nano Lett.* **11**, 1906–1912 (2011).
181. McQuaid, R. G. P., Chang, L. W. & Gregg, J. M. The effect of antinotches on domain wall mobility in single crystal ferroelectric nanowires. *Nano Lett.* **10**, 3566–3571 (2010).
182. Whyte, J. R. *et al.* Ferroelectric domain wall injection. *Adv. Mater.* **26**, 293–298 (2014).
183. Whyte, J. R. *et al.* Sequential injection of domain walls into ferroelectrics at different bias voltages: paving the way for “domain wall memristors”. *J. Appl. Phys.* **116**, 066813 (2014).
184. Whyte, J. R. & Gregg, J. M. A diode for ferroelectric domain-wall motion. *Nat. Commun.* **6**, 7361 (2015).
185. McGilly, L. J., Yudin, P., Feig, I. L., Tagantsev, A. K. & Setter, N. Controlling domain wall motion in ferroelectric thin films. *Nat. Nanotechnol.* **10**, 145–150 (2015).
186. Agar, J. C. *et al.* Highly mobile ferroelastic domain walls in compositionally graded ferroelectric thin films. *Nat. Mater.* **15**, 549–556 (2016).
187. Newns, D. M., Elmegeen, B. G., Liu, X.H. & Martyna, G. J. The piezoelectric transistor: a nanoactuator-based post-CMOS digital switch with high speed and low power. *MRS Bull.* **37**, 1071–1076 (2012).
188. Tsybmal, E. Y., Gruverman, A., Garcia, V., Bibes, M. & Barthélémy, A. Ferroelectric and multiferroic tunnel junctions. *MRS Bull.* **37**, 138–143 (2012).
189. Tsybmal, E. Y. & Gruverman, A. Ferroelectric tunnel junctions: beyond the barrier. *Nat. Mater.* **12**, 602–604 (2013).
190. Maksymovych, P. *et al.* Polarization control of electron tunneling into ferroelectric surfaces. *Science* **324**, 1421–1425 (2009).
191. Chanthbouala, A. *et al.* Solid-state memories based on ferroelectric tunnel junctions. *Nat. Nanotechnol.* **7**, 101–104 (2012).
192. Wen, Z., Li, C., Wu, D., Li, A. & Ming, N. Ferroelectric-field-effect-enhanced electroresistance in metal/ferroelectric/semiconductor tunnel junctions. *Nat. Mater.* **12**, 617–621 (2013).
193. Salahuddin, S. & Datta, S. Use of negative capacitance to provide voltage amplification for low power nanoscale devices. *Nano Lett.* **8**, 405–410 (2008).
194. Qi, Y. & Rappe, A. M. Designing ferroelectric field-effect transistors based on the polarization-rotation effect for low operating voltage and fast switching. *Phys. Rev. Appl.* **4**, 044014 (2015).
195. Khan, A. I. *et al.* Experimental evidence of ferroelectric negative capacitance in nanoscale heterostructures. *Appl. Phys. Lett.* **99**, 113501 (2011).
196. Appleby, D. J. R. *et al.* Experimental observation of negative capacitance in ferroelectrics at room temperature. *Nano Lett.* **14**, 3864–3868 (2014).
197. Gao, W. *et al.* Room-temperature negative capacitance in a ferroelectric-dielectric superlattice heterostructure. *Nano Lett.* **14**, 5814–5819 (2014).
198. Khan, A. I. *et al.* Negative capacitance in a ferroelectric capacitor. *Nat. Mater.* **14**, 182–186 (2015).
199. Hong, X., Posadas, A., Zou, K., Ahn, C. H. & Zhu, J. High-mobility few-layer graphene field effect transistors fabricated on epitaxial ferroelectric gate oxides. *Phys. Rev. Lett.* **102**, 136808 (2009).
200. Zheng, Y. *et al.* Gate-controlled nonvolatile graphene-ferroelectric memory. *Appl. Phys. Lett.* **94**, 163505 (2009).
201. Zheng, Y. *et al.* Graphene field-effect transistors with ferroelectric gating. *Phys. Rev. Lett.* **105**, 166602 (2010).
202. Lu, H. *et al.* Ferroelectric tunnel junctions with graphene electrodes. *Nat. Commun.* **5**, 5518 (2014).
203. Song, E. B. *et al.* Robust bi-stable memory operation in single-layer graphene ferroelectric memory. *Appl. Phys. Lett.* **99**, 042109 (2011).
204. Baeumer, C., Rogers, S. P., Xu, R. J., Martin, L. W. & Shim, M. Tunable carrier type and density in graphene/PbZr_{0.2}Ti_{0.8}O₃ hybrid structures through ferroelectric switching. *Nano Lett.* **13**, 1693–1698 (2013).
205. Hong, X. *et al.* Unusual resistance hysteresis in *n*-layer graphene field effect transistors fabricated on ferroelectric Pb(Zr_{0.2}Ti_{0.8})O₃. *Appl. Phys. Lett.* **97**, 033114 (2010).
206. Hinnfeld, J. H. *et al.* Single gate *p*-*n* junctions in graphene-ferroelectric devices. *Appl. Phys. Lett.* **108**, 203109 (2015).
207. Yusuf, M. H., Nielsen, B., Dawber, M. & Du, X. Extrinsic and intrinsic charge trapping at the graphene/ferroelectric interface. *Nano Lett.* **14**, 5437–5444 (2014).
208. Baeumer, C. *et al.* Ferroelectrically driven spatial carrier density modulation in graphene. *Nat. Commun.* **6**, 6136 (2015).
209. Yuan, Y., Xiao, Z., Yang, B. & Huang, J. Arising applications of ferroelectric materials in photovoltaic devices. *J. Mater. Chem. A* **2**, 6027–6041 (2014).
210. Seidel, J. & Eng, L. M. Shedding light on nanoscale ferroelectrics. *Curr. Appl. Phys.* **14**, 1083–1091 (2014).

211. Butler, K. T., Frost, J. M. & Walsh, A. Ferroelectric materials for solar energy conversion: photoferroics revisited. *Energy Environ. Sci.* **8**, 838–848 (2015).
212. Belinicher, V. I. & Sturman, B. I. The photogalvanic effect in media lacking a center of symmetry. *Sov. Phys. Usp.* **23**, 199–223 (1980).
213. Young, S. M. & Rappe, A. M. First principles calculation of the shift current photovoltaic effect in ferroelectrics. *Phys. Rev. Lett.* **109**, 116601 (2012).
214. Young, S. M., Zheng, F. & Rappe, A. M. First-principles calculation of the bulk photovoltaic effect in bismuth ferrite. *Phys. Rev. Lett.* **109**, 236601 (2012).
215. Zenkevich, A. *et al.* Giant bulk photovoltaic effect in thin ferroelectric BaTiO₃ films. *Phys. Rev. B* **90**, 161409 (2014).
216. Fridkin, V. M. & Popov, B. N. Anomalous photovoltaic effect in ferroelectrics. *Sov. Phys. Usp.* **21**, 981–991 (1978).
217. Basu, S. R. *et al.* Photoconductivity in BiFeO₃ thin films. *Appl. Phys. Lett.* **92**, 091905 (2008).
218. Zhang, J. *et al.* Surface, bulk, and interface electronic states of epitaxial BiFeO₃ films. *J. Vac. Sci. Technol. B* **27**, 2012–2014 (2009).
219. Yang, S. Y. *et al.* Photovoltaic effects in BiFeO₃. *Appl. Phys. Lett.* **95**, 062909 (2009).
220. Choi, T., Lee, S., Choi, Y. J., Kiryukhin, V. & Cheong, S. W. Switchable ferroelectric diode and photovoltaic effect in BiFeO₃. *Science* **324**, 63–66 (2009).
221. Yang, S. Y. *et al.* Above-bandgap voltages from ferroelectric photovoltaic devices. *Nat. Nanotechnol.* **5**, 143–147 (2010).
222. Seidel, J. *et al.* Efficient photovoltaic current generation at ferroelectric domain walls. *Phys. Rev. Lett.* **107**, 126805 (2011).
223. Yan, F., Chen, G., Lu, L. & Spanier, J. E. Dynamics of photogenerated surface charge on BiFeO₃ films. *ACS Nano* **6**, 2355–2360 (2012).
224. Bhatnagar, A., Chaudhuri, A. R., Kim, Y. H., Hesse, D. & Alexe, M. Role of domain walls in the abnormal photovoltaic effect in BiFeO₃. *Nat. Commun.* **4**, 2835 (2013).
225. Grinberg, I. *et al.* Perovskite oxides for visible-light-absorbing ferroelectric and photovoltaic materials. *Nature* **503**, 509–512 (2013).
226. Curtarolo, S. *et al.* The high-throughput highway to computational materials design. *Nat. Mater.* **12**, 191–201 (2013).
227. Ceder, G. & Persson, K. The stuff of dreams. *Sci. Am.* **309**, 36–40 (2013).
228. Baek, S. H. *et al.* Giant piezoelectricity on Si for hyperactive MEMS. *Science* **334**, 958–961 (2011).
229. Yuan, Y. *et al.* Efficiency enhancement in organic solar cells with ferroelectric polymers. *Nat. Mater.* **10**, 296–302 (2011).
230. Choi, Y. *et al.* Enhancement of local piezoresponse in polymer ferroelectrics via nanoscale control of microstructure. *ACS Nano* **9**, 1809–1819 (2015).
231. Fu, D. *et al.* Diisopropylammonium bromide is a high-temperature molecular ferroelectric crystal. *Science* **339**, 425–428 (2013).
232. Bennett, J. W., Garrity, K. F., Rabe, K. M. & Vanderbilt, D. Hexagonal ABC semiconductors as ferroelectrics. *Phys. Rev. Lett.* **109**, 167602 (2012).
233. Snaith, H. J. Perovskites: the emergence of a new era for low-cost, high-efficiency solar cells. *J. Phys. Chem. Lett.* **4**, 3623–3630 (2013).
234. Wu, W. *et al.* Piezoelectricity of single-atomic-layer MoS₂ for energy conversion and piezotronics. *Nature* **514**, 470–474 (2014).
235. Zhu, H. *et al.* Observation of piezoelectricity in free-standing monolayer MoS₂. *Nat. Nanotechnol.* **10**, 151–155 (2015).
236. Belianinov, A. *et al.* CuNP₂S₆ room temperature layered ferroelectric. *Nano Lett.* **15**, 3808–3814 (2015).
237. Muller, J. *et al.* Ferroelectricity in simple binary ZrO₂ and HfO₂. *Nano Lett.* **12**, 4318–4323 (2012).
238. Tinte, S., Burton, B. P., Cockayne, E. & Waghmare, U. V. Origin of the relaxor state in Pb(B_{1-x})_{1-x}O₂ perovskites. *Phys. Rev. Lett.* **97**, 137601 (2006).
239. Grinberg, I., Juhas, P., Davies, P. K. & Rappe, A. M. Relationship between local structure and relaxor behavior in perovskite oxides. *Phys. Rev. Lett.* **99**, 267603 (2007).
240. Grinberg, I., Shin, Y. & Rappe, A. M. Molecular dynamics study of dielectric response in a relaxor ferroelectric. *Phys. Rev. Lett.* **103**, 197601 (2009).
241. Takenaka, H., Grinberg, I., Shin, Y.-H. & Rappe, A. M. Computational studies of lead-based relaxor ferroelectrics. *Ferroelectrics* **469**, 1–13 (2014).
242. Nelson, C. T. *et al.* Domain dynamics during ferroelectric switching. *Science* **334**, 968–971 (2011).
243. Gao, P. *et al.* Revealing the role of defects in ferroelectric switching with atomic resolution. *Nat. Commun.* **2**, 591 (2011).
244. Winkler, C. R. *et al.* Accessing intermediate ferroelectric switching regimes with time-resolved transmission electron microscopy. *J. Appl. Phys.* **112**, 052013 (2012).
245. Winkler, C. R. *et al.* Real-time observation of local strain effects on nonvolatile ferroelectric memory storage mechanisms. *Nano Lett.* **14**, 3617–3622 (2014).
246. Jesse, S. & Kalinin, S. V. Band excitation in scanning probe microscopy: sines of change. *J. Phys. D* **44**, 464006 (2011).
247. Evans, P. G. & Sichel-Tissot, R. J. *In situ* X-ray characterization of piezoelectric ceramic thin films. *Am. Ceram. Soc. Bull.* **92**, 18–23 (2013).
248. Do, D. H. *et al.* Structural visualization of polarization fatigue in epitaxial ferroelectric oxide devices. *Nat. Mater.* **3**, 365–369 (2004).
249. Highland, M. J. *et al.* Polarization switching without domain formation at the intrinsic coercive field in ultrathin ferroelectric PbTiO₃. *Phys. Rev. Lett.* **105**, 167601 (2010).
250. Fong, D. D. *et al.* Stabilization of monodomain polarization in ultrathin PbTiO₃ films. *Phys. Rev. Lett.* **96**, 127601 (2006).
251. Hruszkewycz, S. O. *et al.* Imaging local polarization in ferroelectric thin films by coherent X-ray bragg projection ptychography. *Phys. Rev. Lett.* **110**, 177601 (2013).
252. Highland, M. J. *et al.* Equilibrium polarization of ultrathin PbTiO₃ with surface compensation controlled by oxygen partial pressure. *Phys. Rev. Lett.* **107**, 187602 (2011).
253. Grigoriev, A. *et al.* Nanosecond domain wall dynamics in ferroelectric Pb(Zr,Ti)O₃ thin films. *Phys. Rev. Lett.* **96**, 187601 (2006).
254. Jo, J. Y. *et al.* Nanosecond dynamics of ferroelectric/dielectric superlattices. *Phys. Rev. Lett.* **107**, 055501 (2011).
255. Daranciang, D. *et al.* Ultrafast photovoltaic response in ferroelectric nanolayers. *Phys. Rev. Lett.* **108**, 087601 (2012).
256. Wen, H. *et al.* Electronic origin of ultrafast photoinduced strain in BiFeO₃. *Phys. Rev. Lett.* **110**, 037601 (2013).
257. Li, D. *et al.* Direct *in situ* determination of the polarization dependence of physisorption on ferroelectric surfaces. *Nat. Mater.* **7**, 473–477 (2008).
258. Kim, S., Schoenberg, M. R. & Rappe, A. M. Polarization dependence of palladium deposition on ferroelectric lithium niobate (0001) surfaces. *Phys. Rev. Lett.* **107**, 076102 (2011).
259. Kolpak, A. M., Grinberg, I. & Rappe, A. M. Polarization effects on the surface chemistry of PbTiO₃-supported Pt films. *Phys. Rev. Lett.* **98**, 166101 (2007).
260. Saidi, W. A., Martinez, J. M. P. & Rappe, A. M. Strong reciprocal interaction between polarization and surface stoichiometry in oxide ferroelectrics. *Nano Lett.* **14**, 6711–6717 (2014).
261. Garrity, K., Kolpak, A. M., Ismail-Beigi, S. & Altman, E. I. Chemistry of ferroelectric surfaces. *Adv. Mater.* **22**, 2969–2973 (2010).
262. Giocondi, J. L. & Rohrer, G. S. Spatial separation of photochemical oxidation and reduction reactions on the surface of ferroelectric BaTiO₃. *J. Phys. Chem. B* **105**, 8275–8277 (2001).
263. Gregg, J. M. Exotic domain states in ferroelectrics: searching for vortices and skyrmions. *Ferroelectrics* **433**, 74–87 (2012).
264. Naumov, I. I., Bellaiche, L. & Fu, H. Unusual phase transitions in ferroelectric nanodisks and nanorods. *Nature* **432**, 737–740 (2004).
265. Prosandeev, S. & Bellaiche, L. Characteristics and signatures of dipole vortices in ferroelectric nanodots: first-principles-based simulations and analytical expressions. *Phys. Rev. B* **75**, 094102 (2007).
266. Choudhury, N., Walizer, L., Lisenkov, S. & Bellaiche, L. Geometric frustration in compositionally modulated ferroelectrics. *Nature* **470**, 513–517 (2011).
267. Yadav, A. K. *et al.* Observation of polar vortices in oxide superlattices. *Nature* **530**, 198–201 (2015).
268. Liu, S., Kim, Y., Tan, L. Z. & Rappe, A. M. Strain-induced ferroelectric topological insulator. *Nano Lett.* **16**, 1663–1668 (2016).
269. Tan, L. Z. & Rappe, A. M. Enhancement of the bulk photovoltaic effect in topological insulators. *Phys. Rev. Lett.* **116**, 237402 (2016).
270. Roy, A., Bennett, J. W., Rabe, K. M. & Vanderbilt, D. Half-Heusler semiconductors as piezoelectrics. *Phys. Rev. Lett.* **109**, 037602 (2012).

Acknowledgements

L.W.M. acknowledges support from the Army Research Office under grant W911NF-14-1-0104, the US Department of Energy (DOE) under grant DE-SC0012375, the Gordon and Betty Moore Foundation's EPiQS Initiative, under grant GBMF5307, the National Science Foundation under grants DMR-1124696, DMR-1149062 and ENG-1434147, and the Office of Naval Research under grant N00014-10-1-0525. A.M.R. acknowledges support from the DOE under grants DE-FG02-07ER46431 and DE-FG02-07ER15920, the National Science Foundation under grants DMR-1120901, CBET-1159736, NSF DMR-1124696 and CMMI-1334241, and the Office of Naval Research under grants N00014-11-1-0664, N00014-12-1-1033 and N00014-14-1-0761. A.M.R. and his group thank the High-Performance Computing Modernization Office of the Department of Defense and the National Energy Research Scientific Computing program. Both authors have benefited from collaborations within programs at the University of California, Berkeley, the University of Illinois, Urbana-Champaign, and the University of Pennsylvania, as well as other valued collaborators around the world.

Competing interests statement

The authors declare no competing interests.

How to cite this article

Martin, L. W. & Rappe, A. M. Thin-film ferroelectric materials and their applications. *Nat. Rev. Mater.* **2**, 16087 (2016).

FURTHER INFORMATION

Materials Genome Initiative: <https://www.whitehouse.gov/mgi>